Master's thesis in chemistry – molecular modelling

Validation study of ReaxFF-optimized geometries in ruthenium compounds

Mauricio Ayala Ortega

Kjemisk Institutt

Universitetet i Bergen

ACKNOWLEDGMENTS

Prof. Dr. Vidar R. Jensen, for giving me the opportunity to belong to a very nice and dedicated group of chemists, every meeting I learned something new from you, thank you.

Marco Foscato, I will always remember your teaching techniques, thank you for opening the door every time I needed it. I'll do the same for you even if it is just Realfagbygget's door. Abrazo grande a Giulia.

My parents, Mary and Manuel, thank you for all the support and trust. You were fundamental for me to reach where I am.

Itzel, I missed you since day number one, thank you for your support.

Thanks to my sister Erandi, that never gives up, until she reaches the top.

Anu and Binod your company here was a big push for me, thank you for the nice moments.

Chuy, this is for you and all the love you left us.

Wietse, Vitali, Marta, Fredrick, thank you for your nice company and good moments.

Dr. Giovanni Occhipinti and Prof. Dr. Knut Børve, thank you for your help along this two years.

Dr. Tomás Rocha, thank you for your valuable and last-minute comments about the thesis.

The CONACyT and México (Register number: 215885) for providing me with financial support.

Thanks to my friends at Alrek and the Faculty of Chemistry, it was a great experience to share with you and enjoy Norway.

Yousef and Armand, thank you for your friendship and help.

List of abbreviations

ZINDO	Zemmer Intermediate Neglect of Differential Overlap
MLCT	Metal to Ligand Charge Transfer
bpy	bipyridine
ADF	Amsterdam Density Functional
LDA	Local Density Approximation
GGA	Generalized Gradient Approximation
QM	Quantum Mechanics
DFT	Density Functional Theory
WRMSD	Weighted Root Mean Square
MUE	Mean Unsigned Error
MSE	Mean Signed Error
MM	Molecular Mechanics
UFF	Universal Force Field
CSD	Cambridge Structural Database
e_{C-N}	carbon-nitrogen interatomic distance difference between the X-ray-structure and the ReaxFF-energy-minimized-structure.
e_{C-O}	carbon-oxygen interatomic distance difference between the X-ray-structure and the ReaxFF-energy-minimized-structure.
e_{C-C}	carbon-carbon interatomic distance difference between the X-ray-structure and the ReaxFF-energy-minimized-structure.
e_{N-O}	nitrogen-oxygen interatomic distance difference between the X-ray-structure and the ReaxFF-energy-minimized-structure.
e_{Ru-C}	ruthenium-carbon interatomic distance difference between the X-ray-structure and the ReaxFF-energy-minimized-structure.
e_{Ru-O}	ruthenium-oxygen interatomic distance difference between the X-ray-structure and the ReaxFF-energy-minimized-structure.
e_{Ru-N}	ruthenium-nitrogen interatomic distance difference between the X-ray-structure and the ReaxFF-energy-minimized-structure.
R_N	Ratio of nitrogen atoms = number of nitrogen atom over the total number of atoms within a molecule.
R_O	Ratio of oxygen atoms = number of oxygen atoms over the total number of atoms within a molecule.
R_C	Ratio of carbon atoms = number of carbon atoms over the total number of atoms within a molecule.
R_H	Ratio of heteroatoms = number of heteroatoms over the total number of atoms within a molecule.

Table of Contents

1 Summary

Ruthenium compounds are widely used in chemistry, due to their flexibility as reagents and catalysts. Some of them have been widely used in olefin metathesis due to their ability to control selectivity in these reactions in addition to their stability to air and moisture. The applications and design of olefin metathesis have been a part of many theoretical studies, specially DFT (Density Functional Theory). In addition to Quantum Mechanics, the use of Molecular Mechanics methods in ruthenium chemistry is an attractive topic since one of the recent developments ReaxFF allows addressing large systems while keeping while reducing the computational effort.

The present thesis, considers the performance of ReaxFF in the optimization of 786 molecules of known crystallographic structure and 11 models derived from DFT. This is done by using two statistical approaches: weighted Root Mean Square of the Distances (WRMSD) and Interatomic distances through (i) the mean unsigned error (MUE) and (ii) the mean signed error (MSE).

Although most of the interaction distances were reproduced by ReaxFF with sufficient accuracy, several significant anomalies, usually in terms of overestimation of bond length were identified and discussed. The longest overestimations of bond lengths were associated with Ru-N bonds. For some of such compounds the bonding interaction clearly demonstrated that the crystallographic structures were not properly reproduced by ReaxFF, resulting in dissociation of N-based ligands from the metal centre during the geometry optimization. Moreover, the presence of at least one Ru-N interaction seemed to affect values of neighbouring bonds and lead to overestimations of the bond lengths of other types of elements.

Notwithstanding the overall good description of bond lengths by ReaxFF, the analysis highlighted low accuracy issues also with respect to systems, like imidazol-2-ylidene ligands, that are of primary importance in the field of Ruthenium-catalysed olefin metathesis. In particular, imidazol-like moieties present overestimations in the C-N bonds within the ring. Finally, with the aim of improving the accuracy of ReaxFF with respect to this type of chemistry, it was suggested to include specific types of compounds in the improvement of ReaxFF parametrization.

2 Introduction

2.1 Importance of ruthenium in organic reactions

Ruthenium compounds have been widely used in the synthesis of organic compounds due to the widest scope of oxidation states[1–3] , and various coordination geometries in each electron configuration. The lower oxidation states of 0, II, and III, ruthenium complexes normally prefer trigonal-bipyramidal and octahedral structures, respectively[3].

Until 1980s the reported synthetic methods using ruthenium reagents and catalysts were limited to a few reactions which include oxidations with RuO_4[4–6], hydrogenation reactions[6–9] and hydrogen transfer reactions[7–9].

Ruthenium complexes can be roughly divided into five groups according to their surrounding ligands[10]: Oxo, carbonyl, tertiary phosphines, cyclopentadienyl, arenes and dienes. These ligands have proven to serve in reactions like hydrogen abstraction, generation of coordinatively unsaturated species by the liberation of ligands, and stabilization of reactive intermediates. Also important, are *N*-heterocyclic carbenes that have made ruthenium the most promising "olefin-metathesis metal" [11,12].

Ruthenium complexes have a variety of useful characteristics including high electron transfer ability, high Lewis acidity, low redox potential, and stabilities of reactive metallic species such as oxo metals, metallacycles, and metal carbene complexes. Thus, a large number of novel useful reactions have begun to be developed using both stoichiometric and catalytic amounts of ruthenium complexes.

2.2 Ruthenium in olefin metathesis

Olefin metathesis (OM) has became a relevant reaction, since it allows the synthesis of tri- or tretrasubstituted olefins, without generating a by-product or only producing one such as ethylene which can be removed by evaporation[13]. Moreover, olefins are used as raw material for a big number of transformations.

OM may be classified in three categories: cross, ring opening and ring closing metathesis (Figure 1)[14]. In cross metathesis, an appropriate catalyst, transposes C_1=C_2 and C_3=C_4 into C_1=C_3 and C_2=C_4.. Since in

principle all olefin reactions are reversible, it is a key issue for chemists, to design reactions in order to avoid back-tracking.

Ring-closing metathesis is the most widely used, here two terminal alkenes react with the catalyst to generate a cyclic olefin releasing a smaller olefin C_2=C_4 in Figure 1.

Finally, the ring opening metathesis, through which a cyclic olefin reacts with a linear (acyclic) olefin generating an acyclic diene.

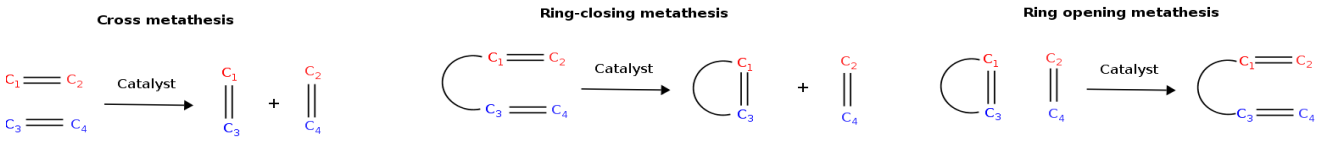

Figure 1: Different types of olefin metathesis. Cross metathesis, ring closing metathesis, and ring opening metathesis

Olefin metathesis mediated by transition metal complexes is an important method. Ruthenium-based catalysts **1**[15–18] and **2**[19] , which are stable to air and moisture, are widely used in OM due to their activity and tolerance of organic functionality.

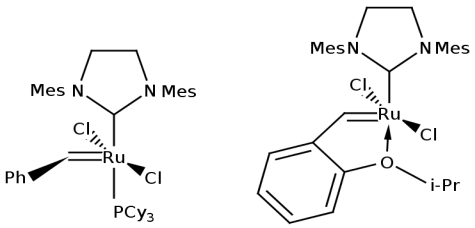

1 **2**

Figure 2: Ru-based catalysts for olefin metathesis reactions where cy=cyclohexyl and Mes= 2,4,6 trimethylphenyl (or mesityl)

While most catalysts favor the formation of the thermodynamically more stable (*E*)-olefins. An important and challenging goal in OM is the development of *Z*-selective catalysts. Recently, in the group, the modification in one step of **2**, has led to remarkable *Z*-selectivity, reaching 96% in metathesis homocoupling of terminal olefins[20].

2.3 Computational studies in olefin metathesis

The Hérisson-Chauvin mechanism of Grubbs catalysts, which fundamental aspects particular to the way in which this class of catalysts mediates olefin metathesis were established by Sanford et al.[21,22]

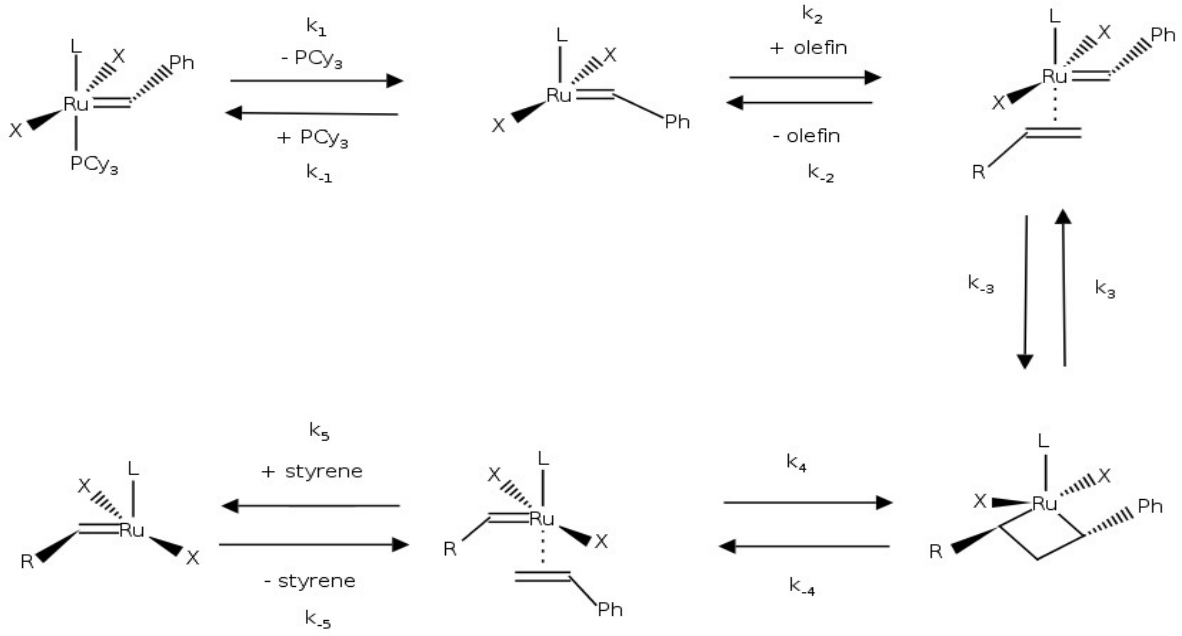

Figure 3: Hérisson-Chauvin Mechanism for Olefin Metathesis Adapted for the Grubbs Ruthenium Catalysts[22]

This work has been used as standard against which to compare experimental[23–38] and computational[39–59] mechanistic contributions.

Density functional theory (DFT) is the preferred computational method in olefin metathesis. The group has contributed with several studies. For instance, comparative studies around Schrock, Fischer carbenes and Grubbs-type olefin metathesis catalysts[60]. A validation study of DFT-optimized geometries of functional transition metal compounds[61]. A Quantitative Structure Activity Relationships (QSAR) of ruthenium catalysts for olefin metathesis[62]. The complete reaction pathway of ruthenium-catalyzed olefin metathesis of ethyl vinyl ether[63].

2.4 Aim of the study

The use of computational and experimental methods in exploring ruthenium chemistry, specially olefin metathesis, has created the interest in the use of empirical methods that include reactivity (reactive force fields), which can contribute in the understanding of ruthenium chemistry, increasing substantially the number of interacting molecules and being computationally economic. ReaxFF could be used for simulating heterogeneous and homogeneous catalysis.

Energy-minimized-structures of the force field, compared with the X-ray and DFT structures through statistical tools like: (i) weighted root mean square of distances WRMSD, and (ii) interatomic distances approach, mean signed error (MSE) and mean unsigned error (MUE), could give an idea of the accuracy of ReaxFF (ruthenium force field) parameters as done previously in the group with the DFT-optimized geometries[61]. The longest errors of these distances (e.g. carbon-carbon, carbon-heteroatom, metal-carbon, and metal-heteroatom) were analysed visually.

3 Theory

3.1 Molecular Mechanics

Molecular mechanics (MM) relies upon laws of classical mechanics, and it uses as a model a molecule which is integrated by atoms (considered as punctual charges with mass) joined by bonds that can be compared with springs. From the use of several parameters like the force constants of bond stretching and the introduction of terms that allow to consider interactions between the non-bonded atoms, the sum of these **eqn.(1)**, constructs an expression for the potential energy that is a function of the atomic positions [65].

$$V = V^{stretch} + V^{angle\,bending} + V^{oop} + V^{torsion} + V^{vdW} + V^{elec} \qquad \textbf{eqn.(1)}$$

These methods consists in analysing the different contributions to the potential energy due to: 1.Bond stretching ($V^{stretch}$), 2. Angle bending ($V^{angle\,bending}$) 3. Out of plane deformation (V^{oop}) 4. Internal rotation around a bond, also called torsion (V^{tor}) 5. Interactions between these class of movements (that produce the cross terms V^{cross}) 6. Attractions and repulsions of van der Waals between the non-

bonded atoms (V^{vdW}) and 7. electrostatic interactions between the atoms (V^{elec}).

MM methods predict equilibrium geometries and relative energies, and are parametrized to be applied to electronic systems in their ground state[66].

The term steric or tension is used by some referring to V, but other authors prefer to use tension energy to denote another quantity[67]. The explicit expressions employed for each term in **eqn.(1)** define what is called force field (FF) in molecular mechanics and the derivatives of the potential energy determine the forces that act in each atom. A force field contains analytical formulas for the terms in **eqn.(1)** as well as the values for all the parameters that appear in these formula.

Molecular Mechanics requires the specification of the atomic coordinates and their connectivity, i.e. the arrangement in which atoms are bonded in a molecule (**Figure 4**). The connectivity should be consistent with the atom types in order to assign the proper parameters and thereby constructing the appropriate potential energy function.

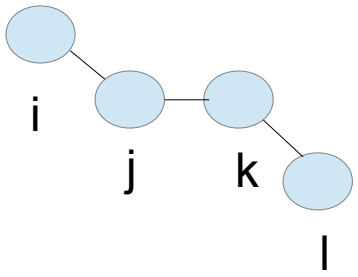

Figure 4: Connectivity in a chemical representation

The different force fields use a set of adjustable parameters, fundamentally force constants, and equilibrium geometries used to calibrate the corresponding force fields.

Molecular mechanics pretends that the parameters and the force constants can be transferred from one molecule to the other, which means that they can be used in any environment. In order for a force field to be useful and give trustable results, it is necessary that the force parameters are completely transferable from one molecule to the other. The equilibrium bond distances, bond angles and dihedral angles are calculated for a set of simple compounds, they are fixed, and then transferred for similar, more complex compounds.

3.1.1 Analysis of the potential energy terms

3.1.1.1 Bond Stretching

The potential energy of bond stretching $V^{stretch}$ is taken as the sum of potential energies $V_{ij}^{stretch}$ for each bond stretch in the molecule over all the pair of atoms directly bonded. The simplest choice for modelling the term $V_{ij}^{stretch}$ is the use of the harmonic oscillator where $V_{ij}^{stretch}$ is a quadratic function of the displacement (or stretching of the bond) l_{ij} from the length of reference or natural l_{ij}^0 this is:

$$V_{ij}^{stretch} = \frac{1}{2} k_{ij} (l_{ij} - l_{ij}^0)^2 \qquad \textbf{eqn.(2)}$$

The force constant k_{ij} and the equilibrium bond length l_{ij}^0 nature of atoms i and j.
This equation represents a parabola: if the atoms move away from the equilibrium distance, the energy of the system increases. The force constant is the strength of the spring or the energy cost that implies a deviation from the equilibrium value l_{ij}^0.

3.1.1.2 Angle bending

The potential energy $V^{angle\ bending}$ is due to the deformation of the bonding angles between three atoms, that is considered as the sum of the potential energies $V_{ijk}^{angle\ bending}$ for the deformation of each bonding angle in the molecule where the sum runs over all the bonding angles in the system under study. In this case, the energy associated with the vibration of bond angle opening and closing is calculated. The simplest choice is a quadratic function:

$$V_{ijk}^{angle\ bending} = \frac{1}{2} k_{ijk} (\Theta_{ijk} - \Theta_{ijk}^0)^2 \qquad \textbf{eqn.(3)}$$

where Θ_{ijk}^0 is the reference value for the angle ijk, this means, the value of the angle in the minimum point of energy. The constant k_{ijk} controls the flexibility of the angle that is formed by three atoms directly bonded. These data are also characteristic of the type of atoms involved.

3.1.1.3 Torsion

The term V^{tor} is taken as the sum of the terms V_{ijkl}^{tor} over all the group of atoms with relation i-l (**Figure 4**) . For example, every hydrogen in ethane H_3C-CH_3, has a relation i-l with each one of the hydrogens in the carbons from the right, giving a total of nine terms in the sum of V^{tor} .The energy V_{ijkl}^{tor} is related with the rotation around the bond j-k in a sequence of four atoms i-j-k-l in. The expression used with more frequency for V_{ijkl}^{tor} is the truncated Fourier series:

$$V_{ijkl}^{tor} = \sum_{n=1} A[1+\cos(n\theta-\theta^0)] \qquad \textbf{eqn.(4)}$$

The parameter n determines periodicity. For example, $n=1$ describes a function of period 2 pi, when $n=2$ a function with period pi, and so on. The constants A determine the size of the rotational barrier around the atoms i-j and depend on the type of atoms (in some situations it could be zero). θ is the dihedral angle in the sequence of atoms ijkl.

In the example of ethane, the most stable conformation is the staggered whereas the eclipsed is a local maximum in energy. As the three hydrogen atoms of each carbon are equivalent, there are three equivalent staggered conformation. The same occurs for the eclipsed conformations. Therefore, the Fourier series for the torsion has only terms corresponding to n=3,6,9.... and only these constants A are different of zero.

3.1.1.4 Cross terms

The cross terms V^{cross} in the expression of V represent couplings between the stretching, bending and torsion. E.g. if the bonds C-O and O-H of one bonding angle COH are elongating, then the distance between the atoms in the extremes from the angle COH is increased, making easier the deformation of the angle. To allow these interactions, a cross term for stretching-bending is added and has the shape

$\frac{1}{2}k_{ij}(\Delta l_i+\Delta l_j)\Delta\theta$, where Δl_i, Δl_j and $\Delta\theta$ are deviations from the reference bonds and angles.

3.1.1.5 Electrostatic interactions

The electrostatic term V^{elec} is taken as the sum of the electrostatic interactions that involve all pairs of atoms except from those with i-j or i-k relation, that is atoms with i-l relation or higher. V_{ij}^{elec} is calculated using the expression for the energy of electrostatic (Coulomb) interaction:

$$V^{elec}=\frac{Q_i Q_j}{\varepsilon_0 R_{ij}} \qquad \textbf{eqn.(5)}$$

where ε_0 is the dielectric constant from the medium and R_{ij} is the distance between the atoms.

3.1.1.6 Van der Waals interactions

The van der Waals term usually is taken as the sum of interactions that involve all the possible pair of atoms with 3 or more bonds of distance. The van der Waals and electrostatic interactions between the atoms with a relation i-j and i-k are considered included in an implicit way in the stretching and bending parameters. Each V^{vdW} is the sum of the attraction due to the dispersion London force and Pauli repulsion. The force fields usually calculate the term V^{vdW} as the Lennard-Jones potential:

$$V^{vdW}=\varepsilon\left[\left(\frac{\sigma}{R_{ij}}\right)^{12}-\left(\frac{\sigma}{R_{ij}}\right)^{6}\right] \qquad \textbf{eqn.(6)}$$

where R_{ij} is the distance between the atoms i and j, the parameter ε is the energy value of V^{vdW} in the minimum of the interaction curve and the parameter of the force field σ is the distance for which V^{vdW} is zero.

3.1.1.7 Parametrization

The parameters of the force field in the MM programs are referred to the values of the force constants and the equilibrium geometry. The accuracy of the predictions of a force field depends on the functions that describe the energy as well as its parameters. This parametrization is done in several steps. First, the ideal values are determined by means of an energy penalization due to deviation with respect to experimental or *ab initio* calculations. Then, this set of initial parameters -known as the proof set- is used to minimize the deviations of the molecular properties (see below) predicted by the MM calculations comparing them with the experimental data or the resulting *ab initio* calculations. Furthermore, in an iterative process, the proof set is corrected and compared again with the experimental references until the difference is small.

The used properties in the parametrization of the force field include: molecular structures, conformational energy differences, vibrational frequencies, internal rotation barriers, dipolar moments and intermolecular interactions.

3.1.1.8 Molecular Properties

MM geometry optimization methods begins with an initial geometry and it has the objective of locating a local minima of the potential energy V. V has an analytical expression, the first and second derivatives of V can be evaluated analytically, which makes easier the energy minimization.

The numerical value of the energy of a conformer in its equilibrium geometry does not have a physical meaning by itself. The zero level of V corresponds to the fictional molecule, in which all the bond lengths and angles have their own reference value and where the torsional, the van der Waals and electrostatic interactions are absent. For the same conformer, the different force fields will give different geometries, and steric energies.

The steric energies depend on how the force field was constructed and how it was parametrized. One of the important physical meaning in molecular mechanics lies in the steric energy difference (calculated in the same force field) between two species that have the same number and atom types, also the same number and bond class, in this way the energy difference between conformers can be used in the steric

energy for giving meaning to the difference of energy calculated between: a) different conformers of the same molecule, b)different stereoisomers of one molecule, e.g. *cis* and *trans* 1,2 dichloroethylene; c) differentiated species by the rotation around a bond, e.g. eclipsed and alternated ethane; d) different geometries of the same molecule, e. g., NH_3 pyramidal and plane; e) two isolated molecules and these forming and hydrogen bond. Besides, an steric energy can be combined with energy parameters of empiric bonds to calculate thermodynamic properties in gas phase.

Some of the force fields available in programs that use MM with some other advantages are: the MM2[67] is useful for calculating small compounds; the MM3 can be employed for small organic compounds, polypeptides and proteins[68] and the MM4 is an implemented version for hydrocarbons[4].

The following force fields are employed with frequency for calculating properties of polypeptides, proteins and nucleic acids: AMBER[70–72] counts with a routine with strict convergence criteria that allow refining the energy. CHARMM[73–75]The MMFF94[76] and the CFF93 and CFF94 calculate organic and inorganic compounds from the main group[77]. The UFF is applied to the compounds of all the elements in the periodic table[78].

3.2 Reactive potential

A reactive potential can simulate reactions between particles by representing the bond formation and dissociation between particles. Unlike non-reactive potentials, they are able to simulate transition states and barrier energy in a reaction accurately. However they are computationally more expensive than non-reactive methods. Some of the commonly used reactive potentials are ReaxFF[64] AIREBO[79] , Brenner[80] , Kiefer[81] , Tersoff[82] . In this thesis, ReaxFF method was used.

3.2.1 ReaxFF Force Field description

ReaxFF is a reactive force field technique in which all atomic interactions are bond order dependant. No reaction sites have to be predefined since it can attain a dynamic description of each atomic and molecular interaction. This is done through a detailed parametrization of the atomic, bonding, angle and torsion properties of each particle and interaction within the system, against quantum and experimental data. We are thus able to obtain a highly accurate, reactive, and dynamic model of atomic

systems. The ReaxFF also allows for the simulation of large systems (on the order of thousands of particles) which would be impractical or impossible to simulate using quantum methods. ReaxFF has seen extensive use over the past 13 years; modelling several different types of reactive systems including combustion[83] , catalysis[84], fuel cells[85] and nanotubes[86].

The forces on each atom are derived from the energy expression given in :

$$E_{system} = E_{bond} + E_{\text{over}} + E_{under} + E_{lp} + E_{val} + E_{tor} + E_{vdW} + E_{Coulomb} \qquad \textbf{eqn.(7)}$$

where the partial contributions to the total energy are the bond, over-coordination penalty, and under-coordination stability, lone pair, valence angle, and torsion, and non-bonding Coulombic and van der Waals energies in a self-explanatory notation.

3.2.1.1 Bonded interactions

3.2.1.1.1 Calculating bond order

After the initial positions of each atom in the system are recorded, the first step is to determine the bond order between each atom pair. An example for this bond order calculation for a carbon-carbon interaction is given in **eqn.(8)**:

$$BO_{ij} = \exp\left[P_{bo,1}\left(\frac{r_{ij}}{r_0^{\sigma}}\right)^{P_{bo,2}}\right] + \exp\left[P_{bo,3}\left(\frac{r_{ij}}{r_0^{\pi}}\right)^{P_{bo,4}}\right] + \exp\left[P_{bo,5}\left(\frac{r_{ij}}{r_0^{\pi\pi}}\right)^{P_{bo,6}}\right] \qquad \textbf{eqn.(8)}$$

where three exponential terms: (1) the sigma bond ($P_{bo,1}$ and $P_{bo,2}$) (2) the first pi bond ($P_{bo,3}$ and $P_{bo,4}$) and (3) the second pi bond ($P_{bo,5}$ and $P_{bo,6}$) . Each bonding term, $P_{bo,1}$, $P_{bo,2}$, $P_{bo,3}$, $P_{bo,4}$, $P_{bo,5}$, $P_{bo,6}$ and each bonding equilibrium distance, r_0^{σ} , r_0^{π} , $r_0^{\pi\pi}$ have been parametrized so as to yield bond strength and distances that agree with quantum mechanically predicted values for species that are separated by a r_{ij} distance[71,84,87]. This carbon-carbon interaction is represented graphically in **Figure 5**. This figure highlights three of the main features of using the ReaxFF bond order scheme: (1) there is a smooth/continuous dependence on the distance for each of the single, double, and triple bond types; (2) there is a smooth/continuous transition of the total bond order from a completely non-bonded interaction to a full triple bonded state; (3) bonding interactions begin at a much farther distance than those typically found in other reactive force field methods[80,88–90] . Because of the large distances at which bonded interaction begins, ReaxFF can accurately model the long range, partially bonded

configurations of transition states.

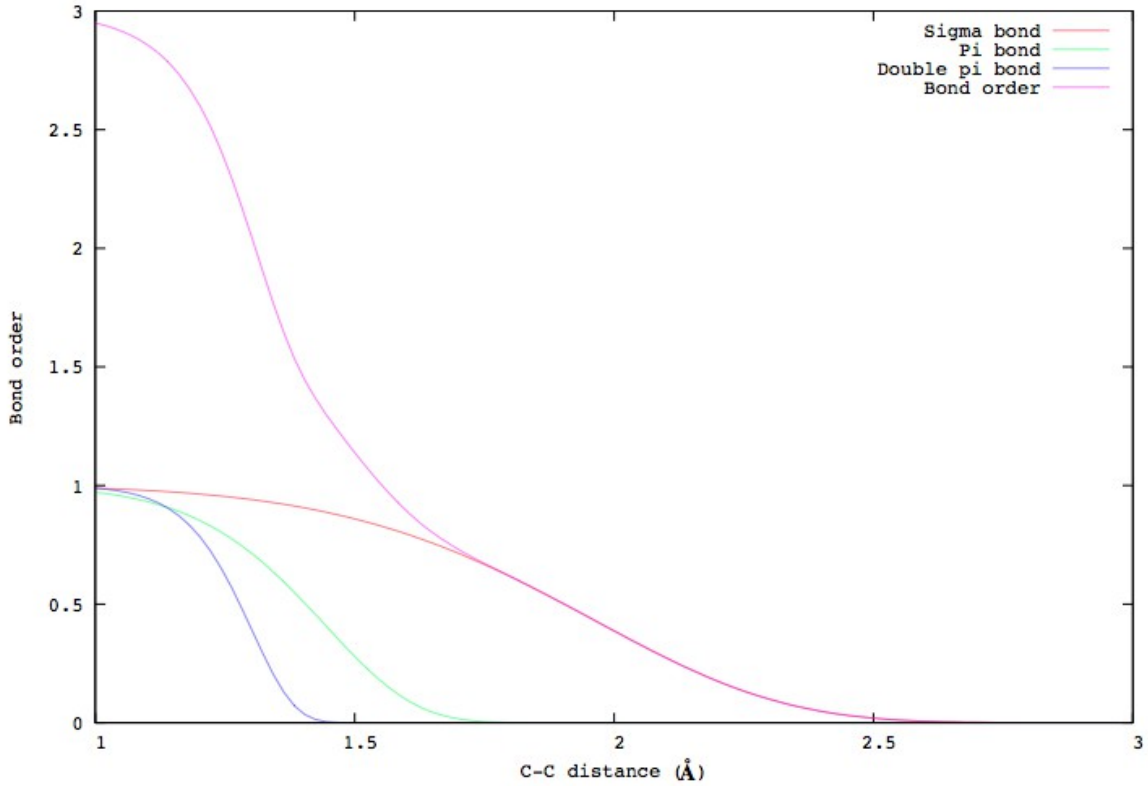

Figure 5: Interatomic distance dependency of the carbon-carbon bond order (the graph was plotted using data from the article: Van Duin, A. C. T.; Dasgupta, S.; Lorant, F.; Goddard, W. A. ReaxFF: A Reactive Force Field for Hydrocarbons. *J. Phys. Chem. A* **2001**, *105*, 9396–9409.)

3.2.1.1.2 Angle and torsion interactions

A disadvantage of force fields is their rigid description of angle and torsion interactions among atoms within the simulation. These types of interactions are usually described with a simple harmonic relationship, and the same harmonic potential applies regardless of how strong or weak a bond gets. In ReaxFF, these angle and torsion interactions are also bond order dependent. This means that as an atom breaks a bond and leaves the molecule, the force exerted on it due to angle and torsion with respect to the rest of the molecule weakens smoothly along with the bond order.

$$E_{angle}=[1-\exp(\lambda\cdot BO_1^3)]\cdot[1-\exp(\lambda\cdot BO_2^3)]\cdot\left(k_a-k_b\cdot\exp\left(-k_b\cdot(\phi-\phi_0)^2\right)\right) \qquad \textbf{eqn.(17)}$$

where BO_1 and BO_2 are the bond orders for each of the two bonds connecting the three atoms within an angle, λ is an angular parameter set to obtain an agreement with quantum values, k_a and k_b are the harmonic force constants that determine the depth and width of the angular potential, respectively, ϕ is the angle, and ϕ_0 is the equilibrium angle.

3.2.1.2 Non-bonded interactions

3.2.1.2.1 Charge polarization

Non-reactive force fields for represent charges (e.g. Amber ff 94) using a restraint electrostatic potential fit (RESP) that depend on molecular conformation, often in significant ways. The ReaxFF is capable of calculating the polarization of charges within molecules. This is achieved by using electronegativity and hardness parameters for each element in the system. These values have also been optimized using quantum mechanical data. **eqn.(18)** illustrates how this polarization is calculated:

$$\frac{\partial E}{\partial q_n} = \chi_n + 2 \cdot q_n \cdot \eta_n + C \cdot \sum_{j=1}^{n} \frac{q_j}{\left(r_{nj}^3 + \left(\frac{1}{\gamma_{nj}} \right)^3 \right)^{\frac{1}{3}}}, \sum_{i=1}^{n} q_i = 0 \qquad \textbf{eqn.(18)}$$

where χ_n, and η_n are respectively the electronegativity and hardness the of the element n, and γ_{nj} is the shielding parameter between atoms n and j. This method is based on the Electronegativity Equalization Method (EEM) and charge equilibration (Qeq) methods[90–92]. These charge values are determined for each time step of the simulation, and are dependent on the geometry of the system.

3.2.1.2.2 Coulomb and van der Waals forces

Because of the rigid connectivity associated with non-reactive force fields, the Coulomb and van der Waals forces are typically only calculated between the atom pairs that do not share a bond or valence angle with one another. Within the reactive environment of ReaxFF, however, the Coulomb and van der Waals forces are calculated between all atom pairs, irrespective of their connectivity. To avoid

excessive repulsive or attractive non-bonded interactions at short distance, both the Coulomb and van der Waals interactions are shielded in ReaxFF. This is achieved through the use of a shielding term, γ.

$$E_{Coulomb} = C \cdot \left[\frac{q_i \cdot q_j}{\left(r_{ij}^3 + \left(1/\gamma_{ij} \right)^3 \right)^{1/3}} \right] \qquad \textbf{eqn.(19)}$$

where q_i and q_j are the charges of the two atoms, r_{ij} is the interatomic distance and γ_{ij} is the shielding parameter mentioned above.

3.3 ReaxFF development and actual state

Simulation methodologies in which QM and MM methods are combined, can be applied for large-scale (millions of atoms) molecular dynamics. The results of molecular dynamics are used to extract a mesoscale description, that is, in modelling properties at much larger scales. ReaxFF has been already developed and validated for complex reactions (including catalysis)[86,93] using B3LYP and X3LYP functionals, while ongoing developments including reactions on Pt, Pt_3Co, Pt_3Ni, PtRu and $BiTeO_x$ surfaces[64].

This progress demonstrates that a wide range of reactions and reactive systems can be described using essentially the same FF. ReaxFF has also been adapted for a parallel environment and fully reactive simulations of around half a billion atoms.

3.4 Molecular geometry optimization

Two of the molecular properties that are obtained directly from a calculation are the energy and the geometry. In general, a calculation begins with an initial geometry, based on geometric data available (bond length tables or through structural determinations like X-ray or neutrons diffraction) and chemical intuition.

A lot of problems in computational chemistry can be solved if a multidimensional function is minimized. The optimization process allows localizing stationary points in a function, for example,

those points where the first derivative of the function is zero. In an optimization of the geometry, stationary points of minimum energy are searched and characterized through the resultant positive-definite Hessian matrix evaluated at the stationary point. In other occasions, for example, when elemental reactions are studied, a chair point, associated with a transition state and that presents a second derivative of negative sign, can be localized.

3.5 Statistical tools and meanings

3.5.1 Error

According to the dictionary of statistical terms[94], the word "error" is used in statistics to denote the difference between an occurring value and its "true" or "expected" value. There is here no imputation of mistake on part of a human agent; the deviation is a chance effect. In this sense, we have, for example errors of observation, errors in equations, errors of the first and second kinds in testing hypothesis, and the error band surrounding an estimate; and also the curve of errors itself.

3.5.2 Mean signed error

The mean signed error is the difference from a set of n pairs, (θ_i', θ) where θ_i' is an estimate of θ, where is expected that $\theta = \theta_i'$. The mean signed error is defined to be:

$$MSE(\phi') = \frac{\sum_{i=1}^{n} \theta_i' - \theta_i}{n} \qquad \textbf{eqn.(20)}$$

3.5.3 Mean unsigned error

The mean unsigned or absolute error is a quantity used to measure how close predictions are to the eventual outcomes. The mean unsigned error is given by:

$$MUE(\phi') = \frac{\sum_{i=1}^{n} |\theta' - \theta_i|}{n} \qquad \textbf{eqn.(21)}$$

The mean absolute error is an average of the absolute errors, where θ_i' is the prediction and θ_i the true value.

3.5.4 Root mean square

A kind of average sometimes used in statistics and engineering, often abbreviated as RMS. To find the root mean square of a set of numbers, square all the numbers in the set and then find the arithmetic mean of the squares. The RMS is the square root of the last result.

$$RMS = \sqrt{\frac{\sum_{i=1}^{n} a_i^2}{n}} \qquad \textbf{eqn.(22)}$$

4 Computational strategy

4.1 ReaxFF basic inputs and outputs

ReaxFF is written in fortran-77, and can be installed in many operating systems (Linux, Windows and Mac). It is divided in 6 parts: reac.f (general MD routines), poten.f (energy equations), ffopt.f (force field optimization), shanno.f (energy minimization), vibra.f (vibrational frequencies), blas.f (BLAS-routines). Program parameters are found in cbka.blk file.

To run the program, the following files are required: geo (input geometry), control (run control parameters), ffield (force field parameters), and exe (Unix-script). According to the job performed by ReaxFF, different output files are produced, the general files are the following: Connecting table (fort.7, fort.8), Trayectory (xmolout), Molecular composition (molfra.out), run.log (generated by exe-script), output geometry in .bgf (fort.90, $DESCRP.bfg), .geo (fort.98, $DESCRP.geo), MOPAC (output.MOP) and .pdb (output.pdb) formats.

4.2 Selection of structures

The X-Ray structures were manually retrieved from the Cambridge Structural Database[95] (CSD) via ConQuest[96] which works with logical operators (molecules that included at least one Ru, C, O, N and H atoms in their structure), giving a total of 2521 molecules. Afterwards these structures were filtered with the following specifications:

- Molecules with one ruthenium atom per molecule (monometalic)
- Determination of x, y, z coordinates
- R factor 0.05
- Not disordered
- Not errors
- Not polymeric

After using the specifications below, 894 molecules were retrieved. Some of them still had no H in the XYZ file, these molecules were filtered[97] in order to remove structures with missing atoms, and molecules which included another elements like boron and phosphorus were manually deleted. This yield a total of 786 XYZ files of ruthenium compounds. The analysis also included 11 XYZ DFT-structures from the Xiaotai Wang mechanism study[98] , giving a total of 797 XYZ files that conformed the **dataset**.

4.3 Geometry optimization

The 786 X-ray and 11 DFT XYZ files were converted to geo format, via the xtob script, and submitted to energy minimization. The routine performed by ReaxFF is the RMSG (Root mean square of the gradient). The end point criterium of the energy change was chosen to be 1 and the maximum number of iterations 5000.

After energy minimization, the energy-minimized-structures were subtracted from the xmolout file (in XYZ format) and submitted systematically by a script to the quatfit[99] and distances_5.py[61] programs. This script also produced the text files with the list of errors, defined as the difference between X-ray and ReaxFF-energy-minimized-structures distances ($e_{C\text{-}C}$, $e_{C\text{-}Het}$, $e_{Ru\text{-}C}$, $e_{Ru\text{-}Het}$) and calculated the MUE and MSE of these.

4.4 Comparison of structures

First, ReaxFF was used to obtain an evaluation of the actual parameters through two qualitative methods, that had been used previously in the group[61] : (i) the weighted root mean square of distances (WRMSD) difference between the ReaxFF-energy-minimized-structures and X-ray sets of Cartesian coordinates done by the quatfit[99] program. A relative weight is assigned to every pair of atoms that is superimposed by the program. The weights are proportional to the inverse of the distance between the atoms, a higher weight force a tighter fit for the pair. The present analysis is unbiased (equal weights have been used for all atom pairs). And (ii) the mean unsigned error (MUE) and the mean signed error (MSE), where all the interatomic distances were included.

$$MUE(ReaxFF)=\frac{2}{N(N-1)}\sum_{i=1}^{N-1}\sum_{j>i}^{N}\left|R_{ij}(ReaxFF)-R_{ij}(X-ray)\right| \quad \textbf{eqn.(23)}$$

$$MSE(ReaxFF)=\frac{2}{N}(N-1)\sum_{i=1}^{N-1}\sum_{j>i}^{N}\left(R_{ij}(ReaxFF)-R_{ij}(X-ray)\right) \quad \textbf{eqn.(24)}$$

where R_{ij} is the interatomic distance between atom pair ij, and N is the number of atoms.

We have analysed the interatomic distances from the following atom pairs: carbon-carbon, carbon-nitrogen, carbon oxygen, nitrogen-oxygen, ruthenium-carbon, ruthenium-nitrogen, and ruthenium-oxygen choosing a threshold that focused the analysis in the bonded pairs. Having as a base, the X-ray structure. as follows: (1) carbon-carbon distances lower than 1.60 Å, (2) carbon-oxygen distances lower than 1.8 Å, (3) carbon-nitrogen distances lower than 1.8 Å, (4) ruthenium-carbon distances lower than 2.3Å, (5) ruthenium-nitrogen distances lower than 2.3Å, and (6) ruthenium-oxygen distances lower than 2.4 Å.

4.5 Superposed structures

The superposed chemical structures shown in the figures throughout this thesis, were fitted using the quatfit program. A weight of 1 x 10^9 was used in ruthenium atom, so ruthenium atoms had the same coordinates.

5 Results and discussion

5.1 The Cartesian coordinates approach

In order to show and understand the behaviour of the WRMSD values, the frequency of appearance (in intervals of **0.1Å**) of these was plotted. The result is a right tailed distribution (**Figure 6**) whose mean is **0.384 Å** reflecting a good description of most of the structures considered in the analysis. When the WRMSD value increased, the frequency of the values decreased.

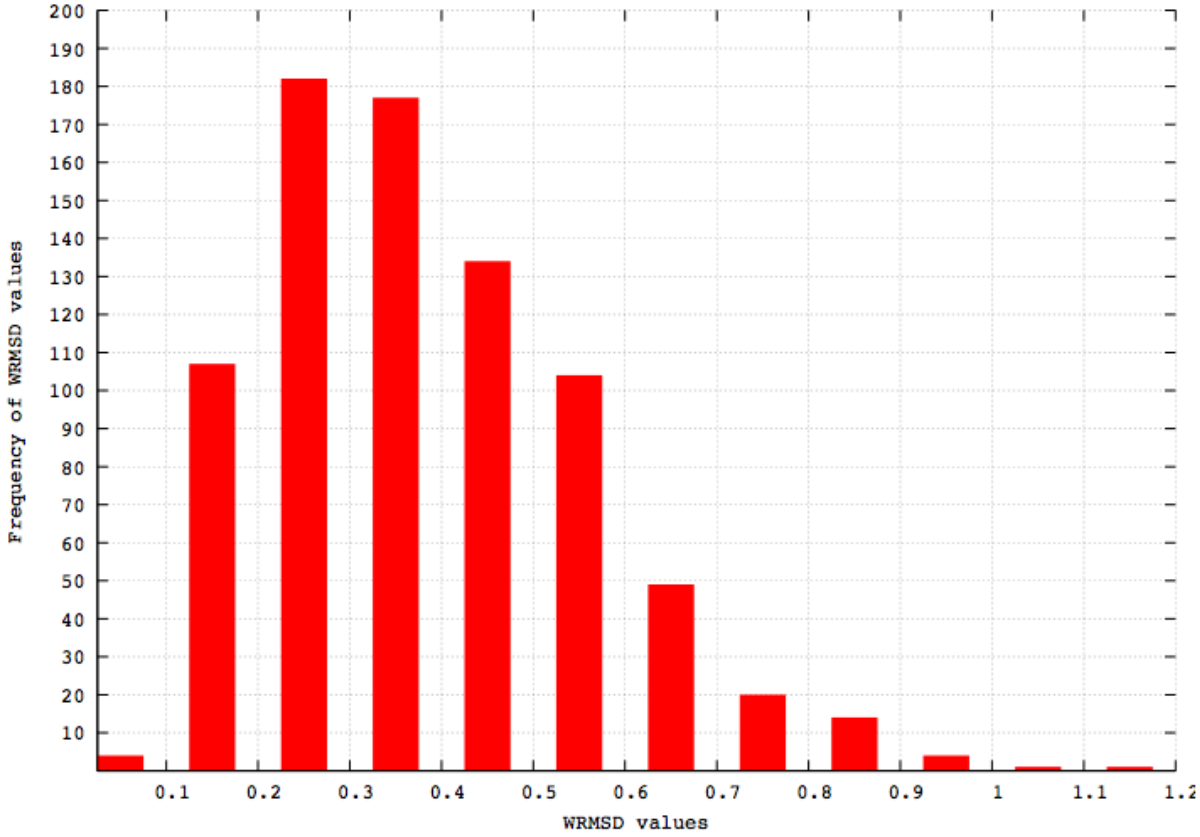

Figure 6: WRMSD (Weighted Root Mean Square Distance) distribution of the dataset. The mean was found in **0.384 Å**.

In the tail of this distribution, the highest WRMSD values (**1.16Å**, **1.00 Å**) belong to the structures shown above (**Figure 7** and **Figure 8**). Both structures showed an overestimation of the ruthenium-nitrogen distances of **2.08Å** to **3.18Å** with respect to the X-ray structure, the nitrogen-hydrogen distances from diazole ring were overestimated from **1.015 Å** to **1.465 Å**, as well as one of the **N-C-C** angle in the diazole ring was underestimated by **9.3º**. Similar chemical structures, with 5 or 6

ruthenium-nitrogen interactions, were found along the longest values in the tail (0.8 Å - 0.7 Å).

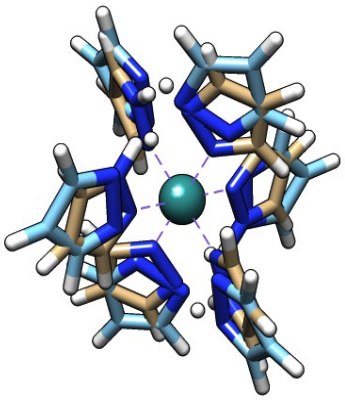

Figure 7. Molecular structure with the **AQIHEO** CSD code. This structure has an RMSD value of 1.00Å. Colour code: X-ray structure carbon atoms brown, ReaxFF-energy-minimized structure carbon atoms (light blue), nitrogen atoms (blue) and hydrogen atoms (white).

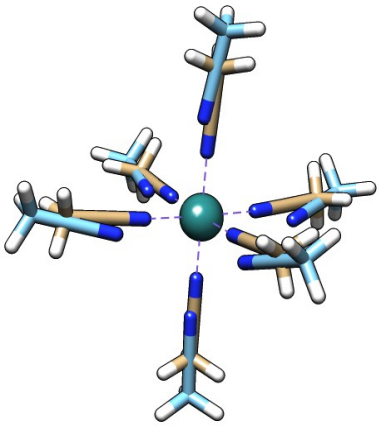

Figure 8 Molecular structure with the **PUHSOB** CSD code. This structure has the highest RMSD value (1.16 Å). Colour code: X-ray structure carbon atoms brown, ReaxFF-energy-minimized structure carbon atoms light blue, nitrogen atoms blue, and hydrogen atoms white.

5.2 The interatomic distances approach

The analysis was performed computing interatomic distances, from X-ray structures and ReaxFF-energy-minimized-structures, the difference between these distances was evaluated statistically via the MUE and MSE, and classified according to the atoms involved on them: carbon-carbon, carbon-nitrogen, carbon-oxygen, nitrogen-oxygen, ruthenium-carbon, ruthenium-oxygen, and ruthenium-nitrogen ($e_{C\text{-}C}$, $e_{C\text{-}N}$, $e_{C\text{-}O}$, $e_{N\text{-}O}$, $e_{Ru\text{-}C}$, $e_{Ru\text{-}O}$, $e_{Ru\text{-}N}$). The approach is intended to understand how well the different interactions are reproduced by ReaxFF[64] (Ruthenium Force Field) actual parameters. This is done by calculating the deviations of interatomic distances with thresholds that account for bonded atoms (information obtained qualitatively in the MUE and MSE errors). We knew in advance that the long distances will dominate the errors over the short or bonded distances[61]. The MUE is calculated from the absolute values of the interatomic distances differences, and it represents the total amount of these differences. There are three possible scenarios for comparing the MUE and MSE values: (1) when the MUE and MSE have the same values, then all the distances are overestimated, (2) when the MUE is higher than the MSE, and the MSE is positive, it is possible to identify that some of the values

were underestimated and most of them were overestimated, and (3) when the MSE has a negative value, most of the values are underestimated and less of them are overestimated.

5.2.1 MUE and MSE of all the stuctures distances

The ruthenium-nitrogen distances (**Figure 9**) were all overestimated (reflected in the MUE and MSE values 0.045 Å), this supports the WRMSD analysis, where it was observed that the structures in the tail of the distribution had ruthenium-nitrogen overestimations. Most of the ruthenium-oxygen distances, which MSE value is negative (-0.148Å) were underestimated (MUE=0.167Å), and the ruthenium-carbon distances were over and underestimated (MUE=0.29Å MSE=0.17Å).

Among the carbon-carbon, carbon-heteroatom MUE and MSE values obtained in this work (**Figure 9**), the e_{C-O} were the ones with the highest values of both MUE = 0.084 Å and MSE = 0.078 Å, followed by e_{C-C} (MUE = 0.046Å and MSE = 0.041Å) and e_{C-N} (MUE = 0.045Å and MSE = 0.01Å). The $\mathbf{e_{N-O}}$ have a MUE of 0.074Å and MSE of 0.050Å.

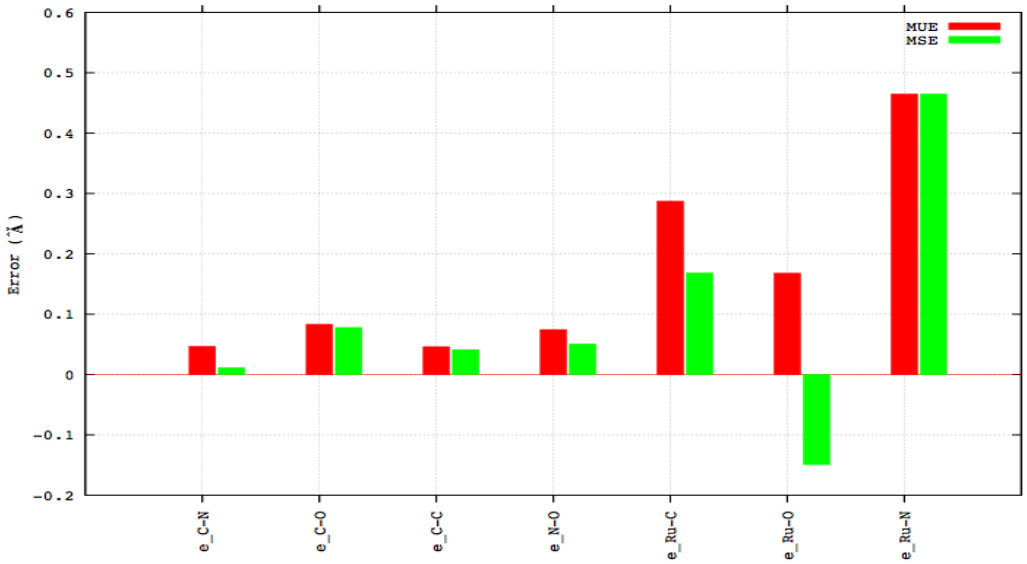

Figure 9: Mean unsigned error (MUE) and mean signed error (MSE) for 4968 C-N distances, 1625 C-O distances, 18723 C-C distances, 172 N-O distances, 3365 Ru-C distances, 471 Ru-O distances, 2057 Ru-N distances

5.2.2 MUE and MSE values of all individual structures

The sorted MUE and MSE values of the individual molecules are shown in **Figure 10**, the highest MUE and MSE values belong to the same structures shown previously in the WRMSD study (**Figure 7** and **Figure 8**) that is chemical structures with either ligands like diazole or acetonitrile or several ruthenium-nitrogen interactions (**Figure 11**). The **C-N-N** angle formed between the carbon in the substituted position of the pyridine ring and the **N=N** bond was decreased from **113.5º** to **74.66º** and from **110.57º** to **88.8º** among these values were also found ruthenium-cyclopentadienyl structures (**Figure 12**).

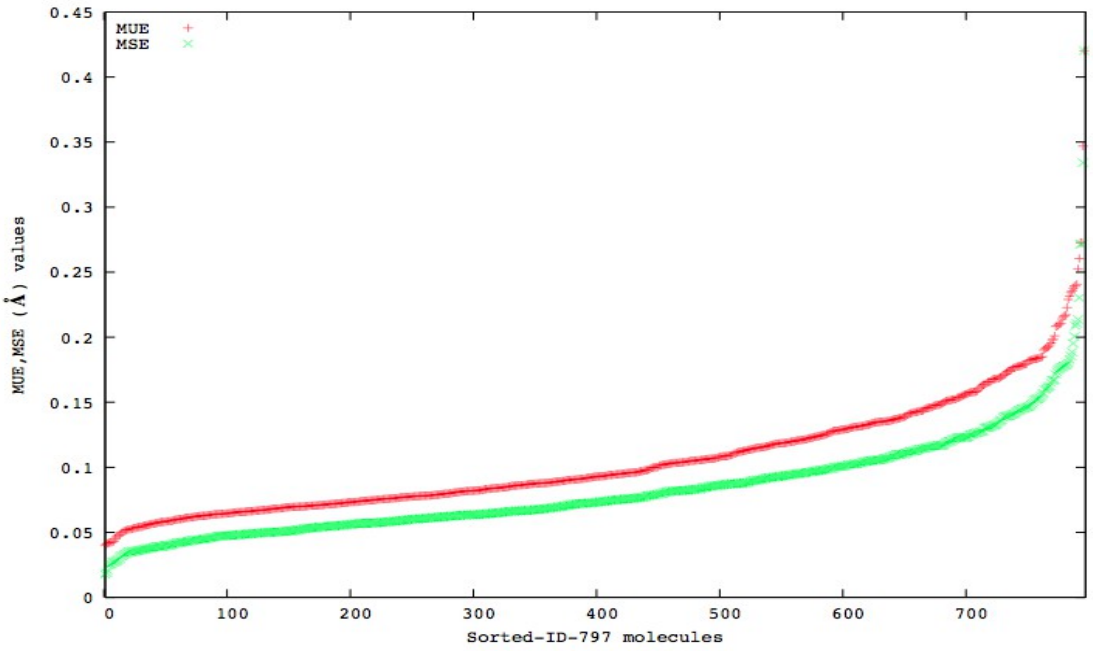

Figure 10 Sorted MUE (red) and MSE (green) individual values of the dataset. The individual MSE and MUE values reflect that MUE and MSE sorted values are close which mean that most of the distances are overestimated and only a few of them are underestimated.

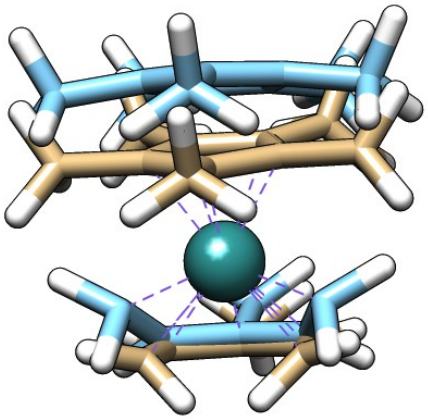

Figure 12 Molecular structure with the **KUCJOH** CSD code This molecule has a MUE value of 0.260Å and MSE value of 0.209Å . Colour code:X-ray structure carbon atoms (brown) ReaxFF-energy-minimized-structure carbon atoms (blue colour) hydrogen atoms white colour.

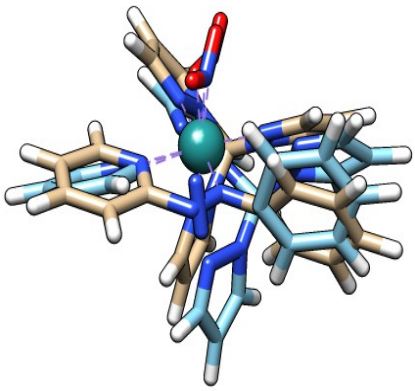

Figure 11 Molecular structure with the **IREGUI** CSD code. MUE value of 0.215Å and MSE value of 0.195Å. Colour code: X-ray structure carbon atoms brown, ReaxFF-energy-minimized structure carbons (light blue). Nitrogen atoms blue colour hydrogen atoms white colour, oxygen atoms red.

5.2.3 MUE and MSE values vs R_{atoms}

The ratio between a certain type of atom/atoms over the total number of atoms within a molecule ($R_{atom/atoms}$) plotted against the MUE/MSE values could offer information about the correlation of these and the MUE/MSE values.

Figure 13 and **Figure 14** present the MUE and MSE as a function of the ratio of the atoms: nitrogen, oxygen, heteroatoms, and carbon atoms (R_N , R_O, R_{Het} and R_C) it is observed that there is no relation between the MUE and MSE values with R_N, R_O, R_{Het} and R_C most of the MUE and MSE values are found below 0.25Å independently from the $R_{atom/atoms}$ values excepting few cases that exceeded this value.

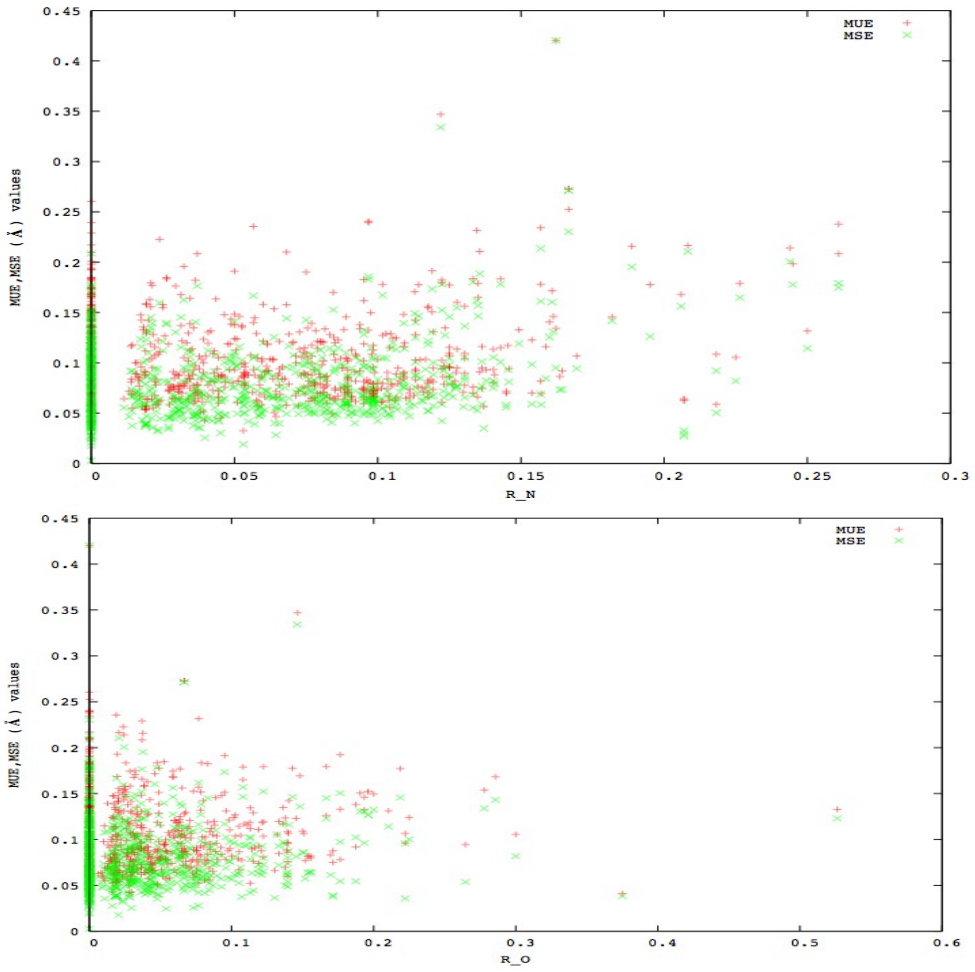

Figure 13: MUE and MSE as a function of the ratio between the atoms of nitrogen and oxygen.

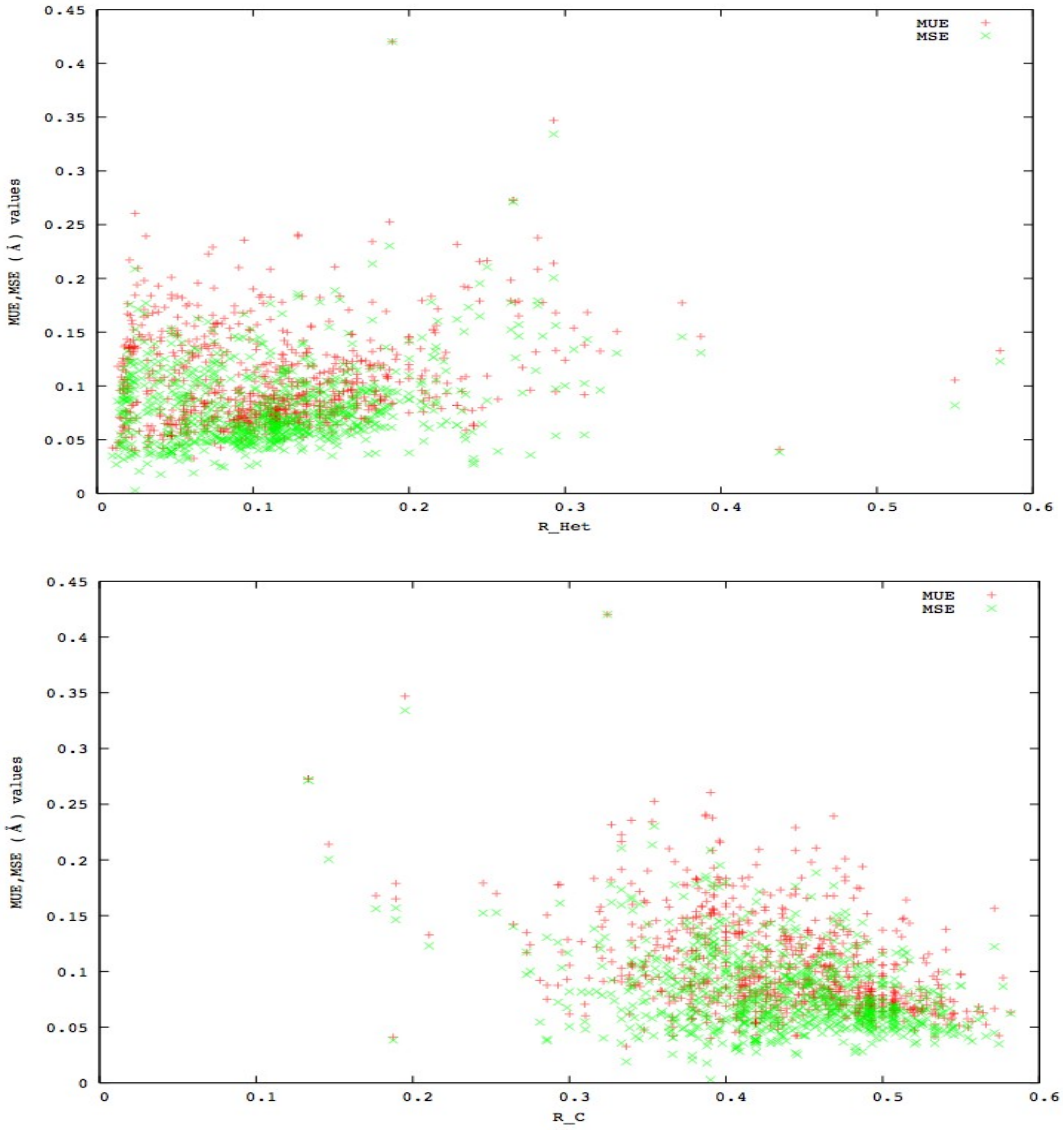

Figure 14 MUE and MSE as a function of the ratio of heteroatoms and carbon atoms

5.2.4 Relation between the e_{C-N} and the number of ruthenium-nitrogen bonds

To complement the ratio study, the carbon-nitrogen and ruthenium-oxygen errors were plotted against the number of ruthenium-nitrogen and ruthenium-oxygen bonds respectively, with the purpose to show whether there was a relationship between the longest overestimations and the number of nitrogen/oxygen atoms within a molecule.

The e_{C-N} showed a slight difference between the values below and above 0.2Å, which are independent of the number of nitrogen atoms within a molecule. The values greater than 0.2Å do not occur very frequently (**Figure 15**).

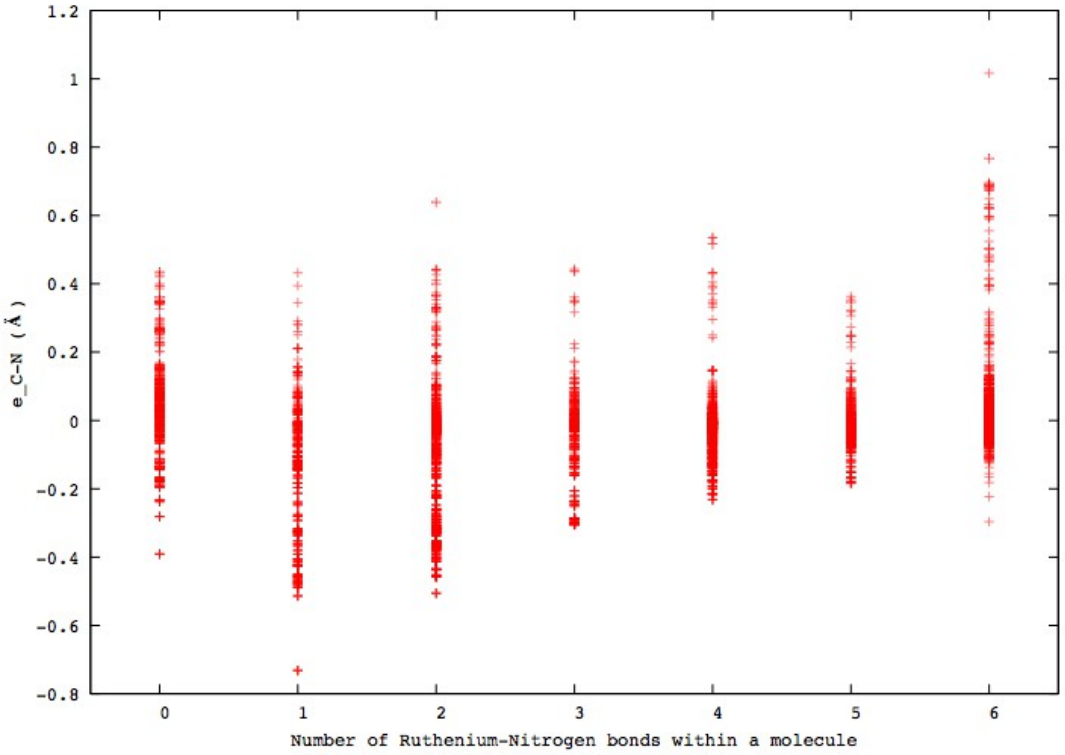

Figure 15 e_{C-N} as a function of ruthenium-nitrogen bonds. Most of the e_{C-N} values are concentrated from -0.1Å to values below 0.2Å. The population of e_{C-N} over 0.2Å is lower. These e_{C-N} are shown in **Figure 16**

The highest overestimations 1.02Å – 0.62Å (A,B,C in **Figure 16)** were related with azo-pyridine, diazole and triazole compounds, where the nitrogen atom of these groups was bonded to the ruthenium atom, below these (**0.42 Å – 0.22 Å**). There were smaller overestimations of $e_{C\text{-}N}$ related with a wide variety of different fragments most of them being aromatic (**D, F, I, J** in **Figure 16**), and metalocylclic (**G, K**) . There were a few exceptions like nitro group in the cyclopentadienyl compound (**E**), and the nitro aliphatics (**H**).

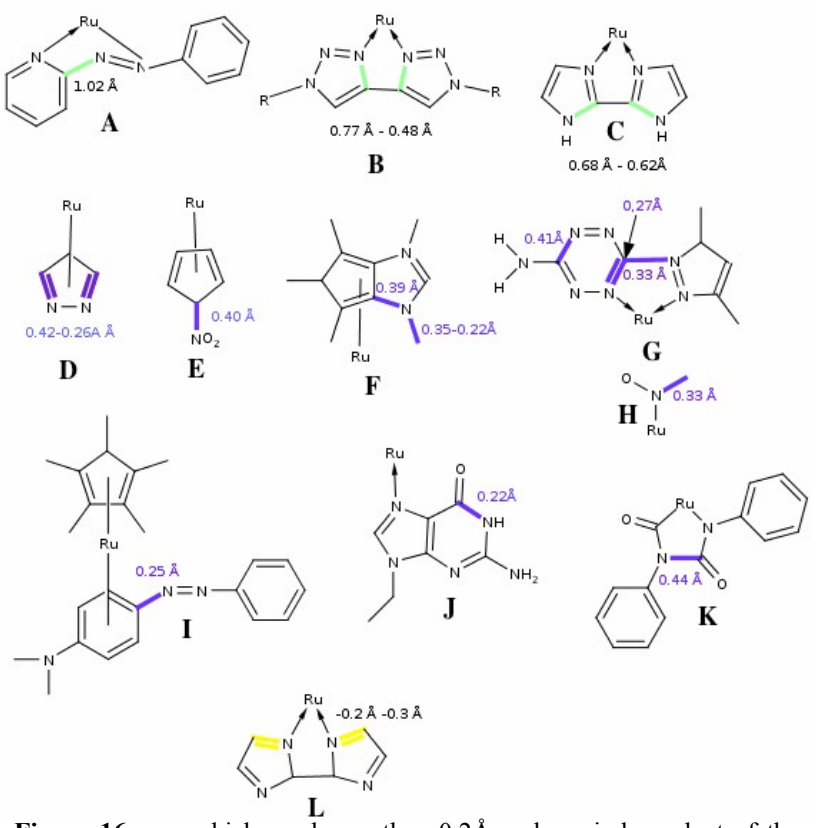

Figure 16. $e_{C\text{-}N}$ which are larger than 0.2Å and are independent of the number of ruthenium nitrogen bonds in the molecule. The colours green, purple and yellow represent errors in the intervals 1.02Å-0.62Å, 0.44Å-0.22Å and -0.2- -0.3Å respectively (**Figure 19**).

5.2.5 Relation between e_{Ru-O} and the number of ruthenium-oxygen bonds.

Similar to the previous analysis, the e_{Ru-O} were plotted against the number of ruthenium-oxygen bonds (**Figure 17**). As the number of ruthenium oxygen bonds is increased within a molecular structure, the e_{Ru-O} are reduced in relative values with respect to these and in some cases they can even be positive (e.g. e_{Ru-O} in **Figure 18**).

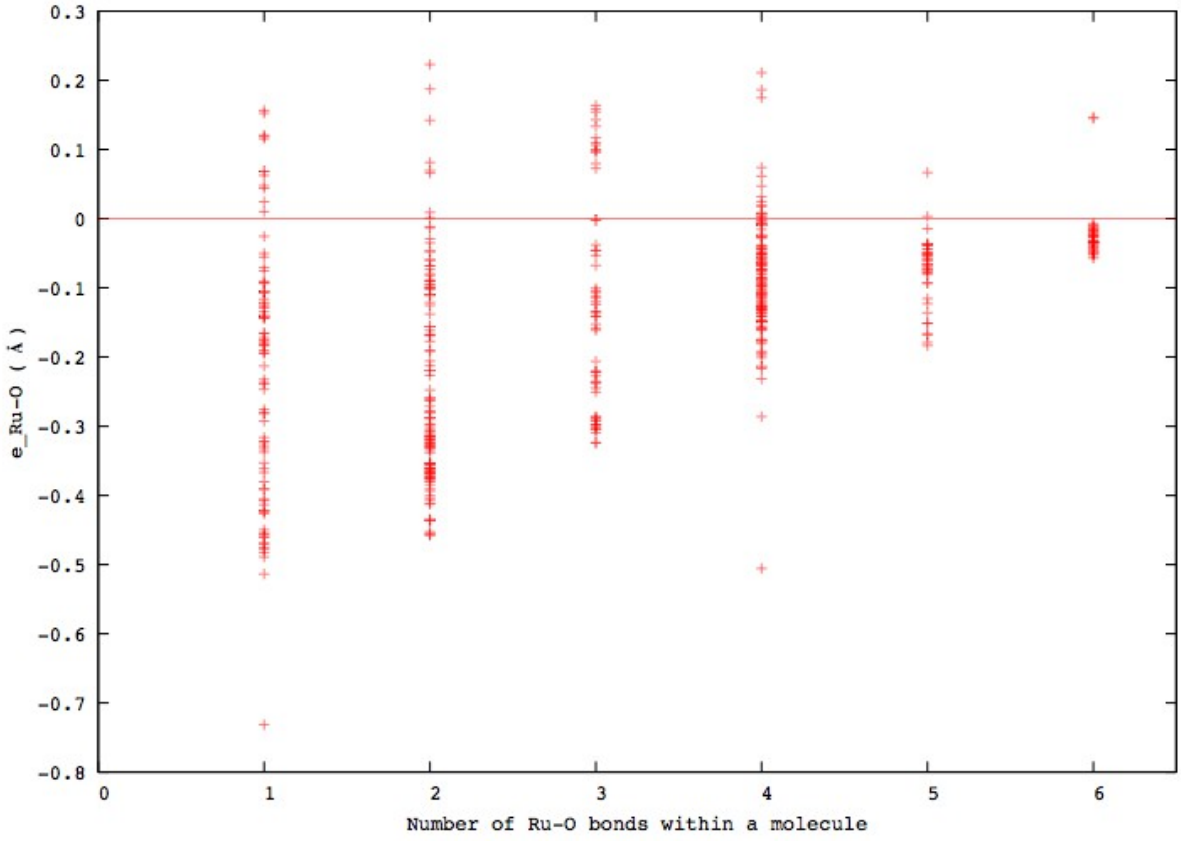

Figure 17 Errors in the ruthenium-oxygen bond lengths as a function of the number of Ru-O within a molecular structure. The errors became narrower and close to zero excepting two errors from the oxalate ligand found in 0.15 Å.

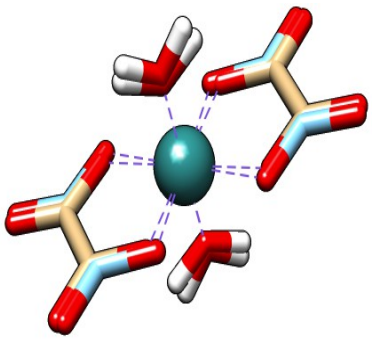

Figure 18 Molecular structure with the **MEMGEQ** CSD Code molecule with 4 e_{Ru-O} from the oxalate ligand in 0.15Å. Colour code: x-ray carbon atoms (brown), ReaxFF-energy-minimized carbon atoms (light blue), oxygen atoms (red), hydrogen atoms white.

5.3 Sorted error plots

The plots of the sorted e_{C-C}, e_{C-Het}, e_{Ru-C}, e_{Ru-Het} and e_{N-O} as a function of the number of distance differences, offers information about the longest overestimations, lowest underestimations, and the bond lengths that ReaxFF describes correctly.

5.3.1 Carbon-nitrogen

As the WRMSD analysis showed, in **Figure 11**, the longest overestimation from e_{C-N} belonged an azo-compound **A.1** bonded to an aromatic and heteroaromatic ring (**1.02 Å**). Below this value, we found overestimations of heteroaromatic ligands like diazole and triazole (**0.77 Å – 0.62 Å**) **A.2** in **Figure 20** and **A.3** in **Figure 21** in which nitrogen atom were bonded to ruthenium atom (green colour). Overestimations from the same kind of ligands, but with carbon atom (from carbene) bonded to ruthenium atom (**0.42 Å-0.46 Å**) were found below. **A.6, A.5, A.7 and A.8** showed chemical structures where every kind of e_{C-N} is related with the colour in the graph.

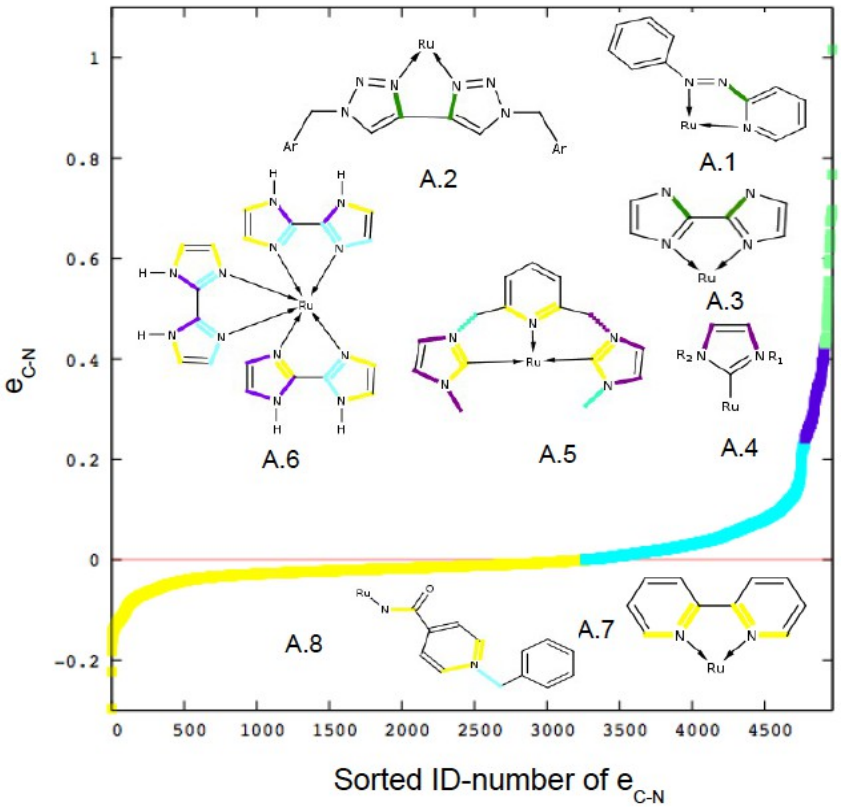

Figure 19: 4975 sorted carbon-nitrogen distances errors from the dataset. 8 fragments are shown to illustrate the most common features in each region, green (1.02Å-0.62Å), purple (0.44Å-0.22Å), light blue (values below 0.2Å and higher than zero) and yellow (negative values).

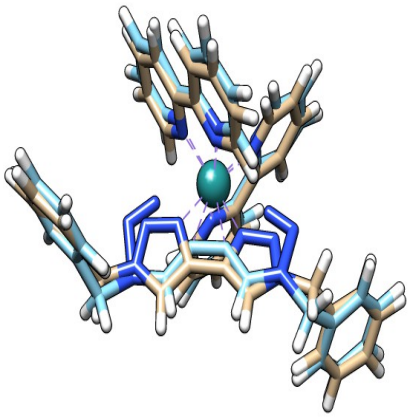

Figure 20: Molecular structure with the **NEGSOJ** CSD Code. Colour code:X-ray carbon atoms (brown colour) ReaxFF-energy-minimized-structure carbon atoms (light blue colour) niitrogen atoms (blue colour) ruthenium atoms (green colour).

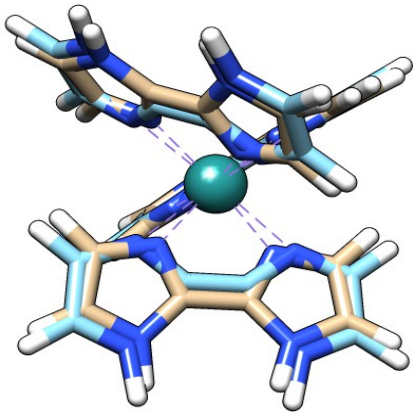

Figure 21: Molecular structure with the **NUCFOH** CSD code. Colour code: X-ray carbon atoms (brown colour) ReaxFF-energy-minimized-structure (light blue colour) nitrogen atoms (blue colour) ruthenium atoms (green colour).

5.3.2 Carbon-oxygen

The largest overestimations for the $e_{C\text{-}O}$ were related with O atoms bonded to an aromatic moiety e.g. **B.1** in **Figure 23** and **B.2** in **Figure 24** and **Figure 25.** In these cases it was also noted that nitrogen atom was bonded to ruthenium atom. Just like in the longest carbon-nitrogen overestimations. After these, the largest C-O overestimation is related to a carboxylic group bonded to two diazole rings **B.3** in, $e_{C\text{-}O}$ from the same functional group, bonded to pyridine were found below this value, where nitrogen atom from the heteroaromatic system was bonded to ruthenium atom **B.4**. The $e_{C\text{-}O}$ decreased when the oxygen were substituted in aromatic systems **B.5**,**B.6**. As the number of oxygen atoms increased within the same molecule (**B.6**, **B.7**), the carbon-oxygen errors decreased even more. Finally the $e_{C\text{-}O}$ from the carbonyl group directly bonded to ruthenium were the best estimations **B.9**.

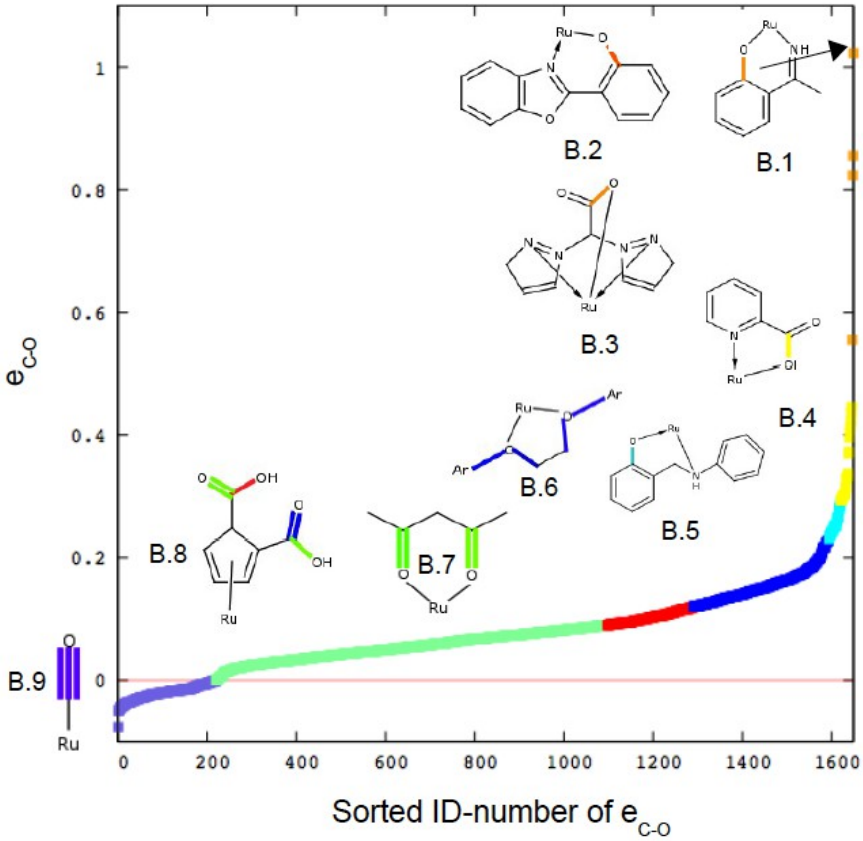

Figure 22: 1649 sorted $e_{C\text{-}O}$ from the dataset. Most of the $e_{C\text{-}O}$ were found between 0 and 0.2Å, 8 fragments are shown, in which the C-O bonds are displayed with the colours used in the region, **B.1**, **B.2**, **B.3** (orange) belonged to heteroaromatic and imine ligands bonded to ruthenium as well as phenolic and carboxilic oxygen.

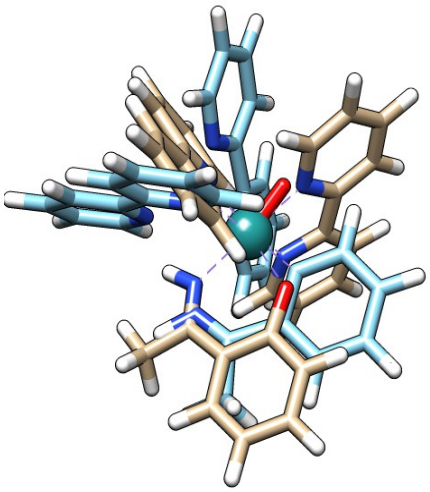

Figure 23: Molecular structure with the **SUXTEK** CSD code. Example of the **B.1** fragment. Colour code: X-ray carbon atoms (brown colour) ReaxFF-energy-minimized structure carbon atoms (light blue colour) oxygen atoms (red colour),nitrogen atoms (blue colour) hydrogen atoms (white).

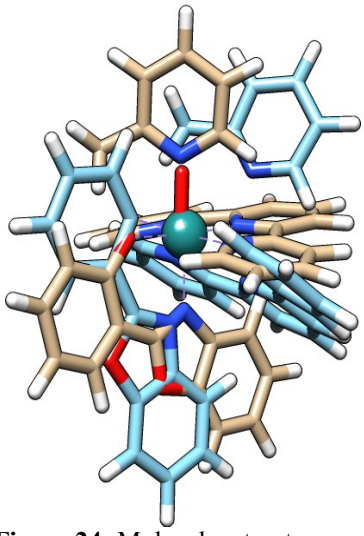

Figure 24: Molecular structure with the **LONVIX** CSD code. Example of the **B.2** fragment Colour code: X-ray carbon atoms (brown) ReaxFF-energy-minimized-structure carbon atoms (light blue) oxygen atoms (red colour) nitrogen (blue colour) hydrogen atoms (white).

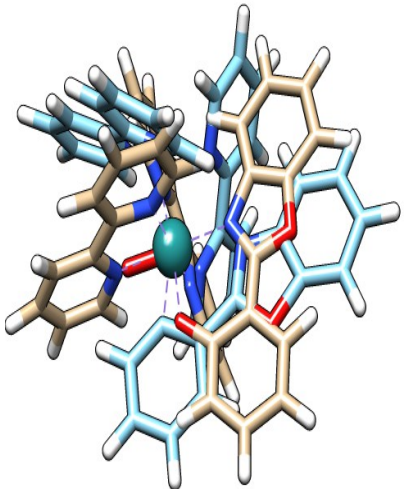

Figure 25: Molecular structure with the **QACYAV** CSD code. Example of the **B.2** fragment. Colour code: X-ray carbon atoms (brown) ReaxFF-energy-minimized structure carbon atoms (light blue) oxygen atoms (red) nitrogen (blue) hydrogen atoms (white).

5.3.3 Carbon-carbon

The largest error in the calculation of the C-C bond found in carbon atoms bridging two nitrogens (from a cyclic diimine **C.1** in **Figure 27**), secondary amines (**C.4** in **Figure 31** and **C.5** in **Figure 30)** or C atoms of carbonyl groups substituting the para position in the pyridine ring of (**C.3** in **Figure 28**). Apart from this pattern, the $e_{C\text{-}C}$ in **1.50 Å** belonged to an oxalate ligand (**C.2** in **Figure 29**). Below these overestimations, **0.44Å-0.19Å** $e_{C\text{-}C}$ of cyclopentadienyl compounds (**C.8**), as well as heteroaromatic compounds like pyridine ring, were observed. The smallest overestimations of the C-C bonds were found for heterocyclic, aromatic and cyclopentadienyl compounds. The same C-C bond length was underestimated in several substitution positions, alkenes and ethers.

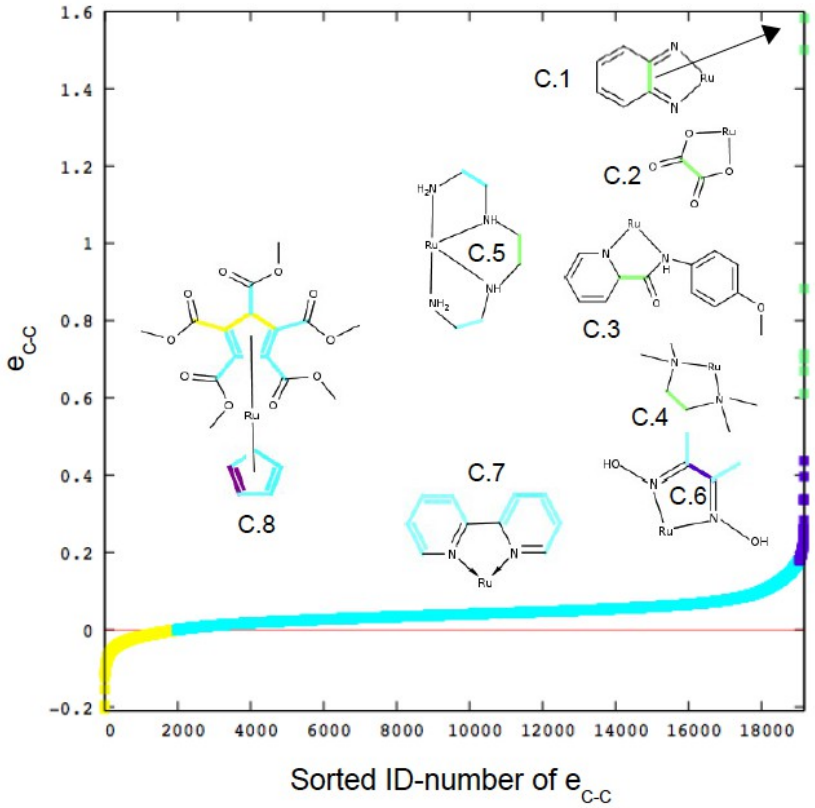

Figure 26: Sorted 19170 carbon-carbon errors from the dataset. 8 fragments are shown, relating the colour of the $e_{C\text{-}C}$ in the fragments and the colour in the region. The longest overestimations (green colour) were found bridging two nitrogens which were also bonded to ruthenium excepting **C.2** $e_{C\text{-}C}$ from an oxalate ligand.. Most of the $e_{C\text{-}C}$ had a good estimation by ReaxFF (ruthenium force field) after energy minimization.

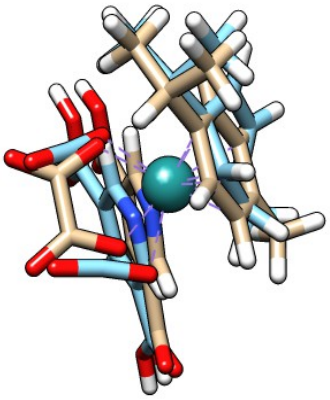

Figure 29: Molecular structure with the **UCOFAU** CSD code. Example of the **C.2** fragment. Colour code: X-ray structure carbon atoms (brown colour) ReaxFF-energy-minimized-structure carbon atoms (light blue) nitrogen atoms (blue) oxygen atoms (red)

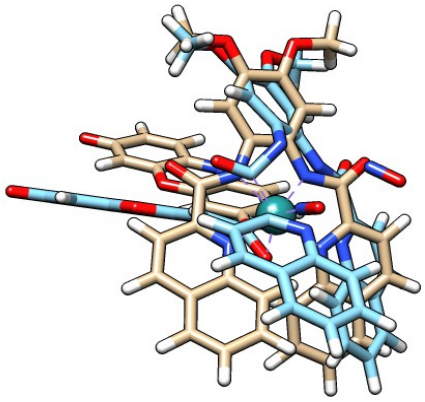

Figure 28: Molecular structure with the **COGXUS** CSD code. Example of the **C.3** fragment. Colour code: X-ray structure carbon atoms (brown) ReaxFF-energy-minimized-structure carbon atoms (light blue) nitrogen atoms (blue) oxygen atoms (red)

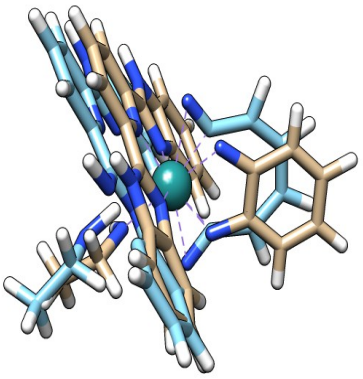

Figure 27: Molecular structure with the **SOMNIS** CSD code. Example of the **C.1** fragment. Colour code: X-ray carbon atoms (brown), ReaxFF-energy-minimized-structure (light blue) nitrogen (blue)

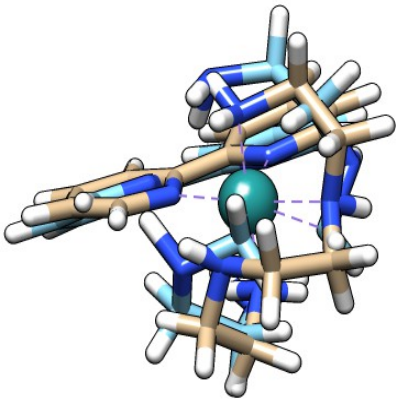

Figure 30: Molecular structure with the **WEMFOK** CSD code. Example of the **C.5** fragment. Colour code: X-ray structure carbon atoms (brown) ReaxFF-energy-minimized-structure carbon atoms (light blue) nitrogen atoms (blue)

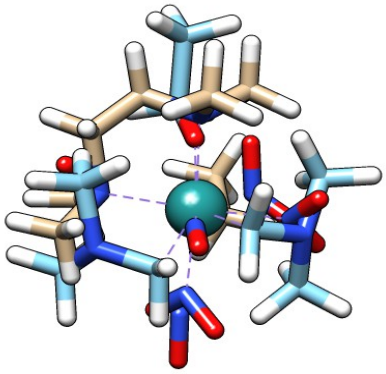

Figure 31: Molecular structure with the **AFAVEI** CSD code. Example of the **C.4** fragment. Colour code: X-ray structure carbon atoms (brown) ReaxFF-energy-minimized-structure carbon atoms (light blue) nitrogen atoms (blue), oxygen atoms (red)

5.3.4 Nitrogen-oxygen

The most numerous N-O bond lengths in the systems under study are related to nitro groups directly bonded to the ruthenium atom. In most of these systems, one of the N-O is underestimated whereas the other N-O is overestimated, **D.1** in **Figure 33** (the one bonded to ruthenium). Another behaviour was observed regarding the N-O bond lengths in nitrate compounds, where 2 bonds were underestimated or, one of them was almost reproduced from the x-ray structure, where as the other was overestimated. The $e_{N\text{-}O}$ in nitrogen monoxide was normally overestimated when it was bonded to ruthenium atom (**D.2** in **Figure 34**).

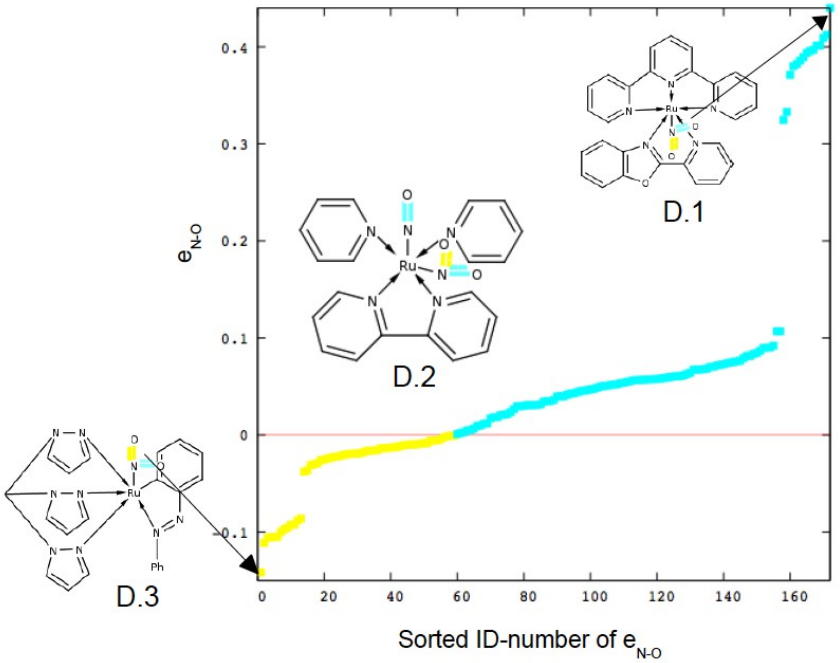

Figure 32:1649 sorted nitrogen-oxygen distances errors from the dataset. 3 molecules are shown, including the largest positive and negative deviations. Most of the nitrogen-oxygen distances belong to nitro groups, nitrate radical, and nitrogen monoxide. Most of the $e_{N\text{-}O}$ reflect a good estimation of ReaxFF-Ruthenium-Force-Field after energy minimization.

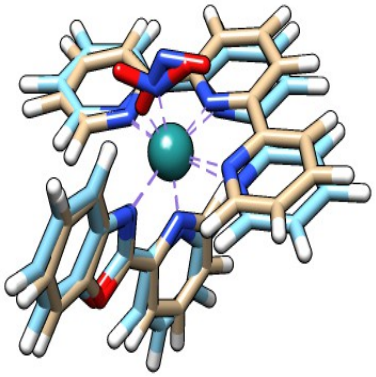

Figure 33: Molecular structure with the **NAPZOU** CSD_code. **D.1** structure. Colour code: X-ray structure carbon atoms (brown) ReaxFF-energy-minimized-structure carbon atoms (light blue) nitrogen atoms (blue) oxygen atoms (red)

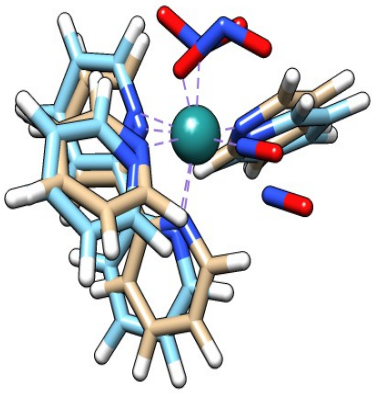

Figure 34: Molecular structure with the **ZIPGEK** CSD code. **D.2** structure. Colour code: X-ray structure carbon atoms (brown) ReaxFF-energy-minimized-structure carbon atoms (light blue) nitrogen atoms (blue) oxygen atoms (red)

5.3.5 Ruthenium-carbon

The largest overestimations for the $e_{Ru.-C}$ are shown in orange colour in **Figure 35** and they correspond to the η^5-cyclopentadienyl compounds. In general, four of the bonds from a cyclopentadienyl ligand were overestimated: two of them higher than the other two (e.g. **1.17Å**, **1.04Å** for the first pair, and **0.63Å**, **0.19Å** for the second **E.1** in **Figure 36** and **E.4**) and one of them almost reproduced. Another feature observed for the same ligands was that one of the two pairs of e_{Ru-C} was overestimated and one or two e_{Ru-C} were underestimated from **-0.1 Å** to **-0.37 Å** (see **E.3).** Purple colour in **Figure 35** the e_{Ru-C} in **1.66 Å** belonged to a carbon (from a carbonyl group, with ruthenium bonded to two cyclooctadiene ligands **E.2** (**Figure 37**))**.** In the case of η^6 aromatic ligands (benzene) two or three e_{Ru-C} were overestimated (close to 0) or underestimated and two e_{Ru-C} were overestimated maximum around **0.64Å** as shown in **E.4 and E.5** in **Figure 35**. e_{Ru-C} from aliphatic-carbons, were almost reproduced and had a maximum e_{Ru-C} of **0.1Å**.

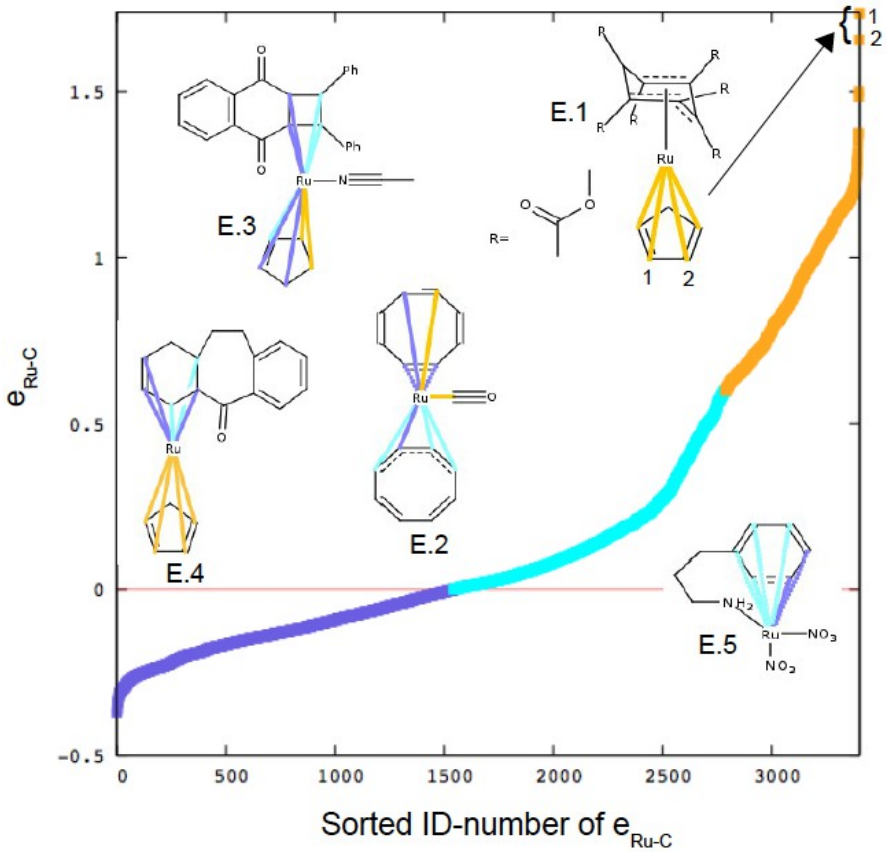

Figure 35: 3403 sorted $e_{Ru\text{-}C}$ from the dataset. Five chemical structures are shown, relating the colour of the $e_{Ru\text{-}C}$ with the , orange colour (largest overestimations) are related with Ru-η^5 cyclopenatdienyl interactions, below (blue colour) Ru-η^6-benzene interactions were found. In purple colour also shown the Ru-η^5 cyclopentadienyl interactions in which two of the $e_{Ru.C}$ were underestimated.

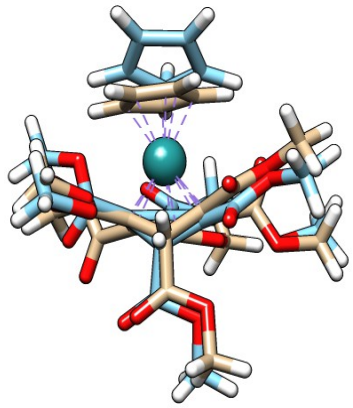

Figure 36: Molecular structure with the **VORHOZ** CSD code. Structure **E.1**. Colour code: X-ray structure carbon atoms (brown) ReaxFF-energy-minimized structure carbon atoms (light blue) oxygen atoms (red)

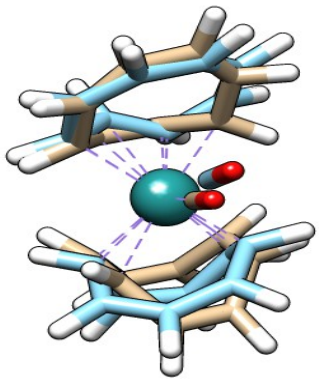

Figure 37: Molecular structure with the **NEHLER** CSD code. Structure **E.2** Colour code: X-ray structure carbon atoms (brown) ReaxFF-energy-minimized structure carbon atoms (light blue)

5.3.6 Ruthenium-oxygen

Most of the e_{Ru-O} were underestimated (yellow colour in **Figure 38**). The largest underestimation (**-0.73 Å**) **F.8** corresponded to a heterocyclic ligand with oxygen substituting the nitrogen position **Figure 39.** β-diketones e_{Ru-O} were almost reproduced **F.5**, as well as water, ethers and esthers **F.7.** The ligands with the highest deviations (cyan color in **Figure 38**), are in the carboxylic groups having one terminal oxygen bonded to ruthenium **F.6**. The largest overestimation value (**0.22 Å**) corresponds to a ruthenium-oxygen distance from oxalate ligand **F.1** previously found in **Figure 29**. If the same ligand was bonded to a molecule with more ruthenium-oxygen bonds, the e_{Ru-O} were underestimated (**Figure 18**). The Ru-O distance in the ligands **F.3** and **F.4** were overestimated.

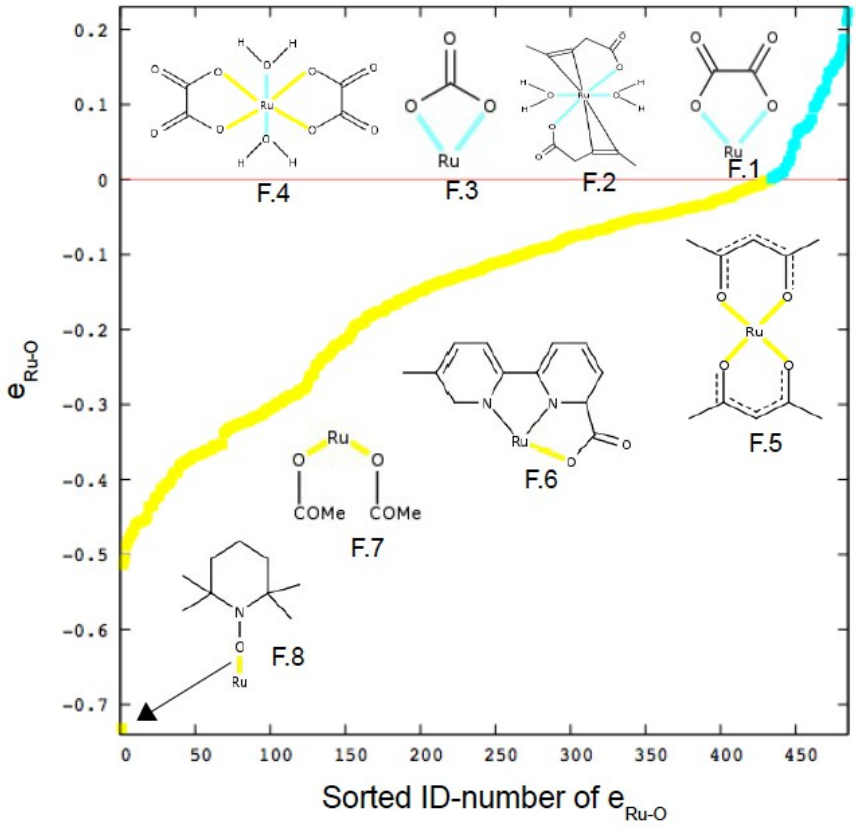

Figure 38: Sorted 485 e_{Ru-O} from the dataset. Most of them were underestimated, 8 fragments are shown, relating the e_{Ru-O} with the colour in the graph. The lowest underestimation **F.8**, belongs to a heterocyclic nitrogen structure.

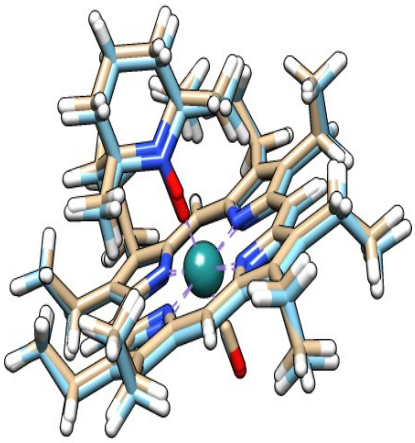

Figure 39: Molecular structure with the **VUPKUM** CSD code. Example of the **F.8** fragment. Colour code: X-ray structure carbon atoms (brown) ReaxFF-energy-minimized-structure (light blue) nitrogen (blue) oxygen (red)

5.3.7 Ruthenium-nitrogen

Every $e_{Ru\text{-}N}$ was overestimated (**Figure 40**). The largest overestimations corresponded to nitrogen monoxide and dioxide structures **G.1** and **G.2** in **Figure 41** with deviation in the interval **2.07Å-1.06Å.** The overestimations of the Ru-N bond length in which the nitrogen belongs to an acetonitrile molecule **G.3** in **Figure 42** is located on a similar interval **1.85Å – 0.84Å**. The differences of the Ru-N bond length associated to heteroaromatic compounds (e.g. diazoles) and non-heterocyclic compounds together with aliphatic amines are located in the intervals **0.79 Å-0.18 Å.**

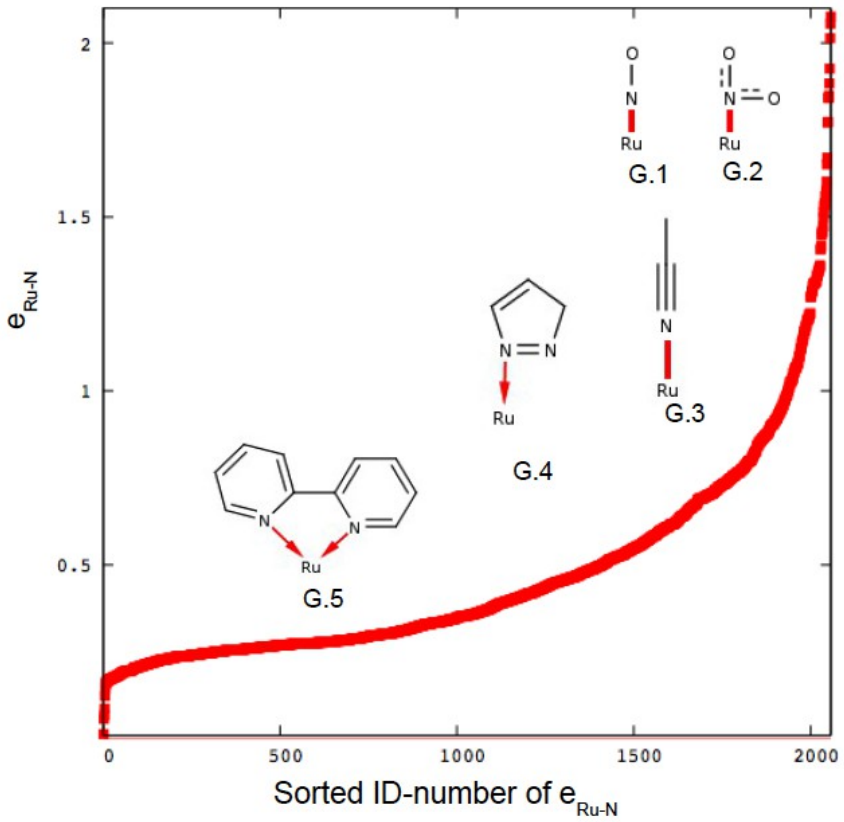

Figure 40: 2057 sorted e_{Ru-N} from the dataset. All Ru-N were overestimated. The largest deviations corresponded to nitro compounds, acetonitrile complexes and diazoheterocyles along with heteroaromatic compounds.

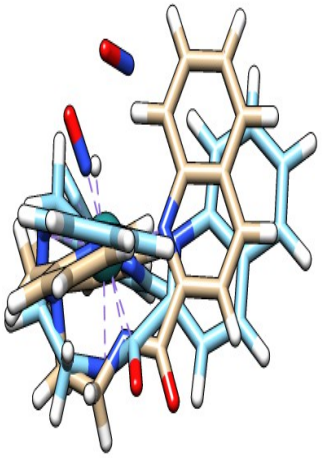

Figure 41: Molecular structure with the **VIKPUB** CSD code. Example of the **G.1** fragment. Colour code: X-ray structure carbon atoms (brown) ReaxFF-energy-minimized-structure carbon atoms (light blue) nitrogen atoms (blue) oxygen atoms (red)

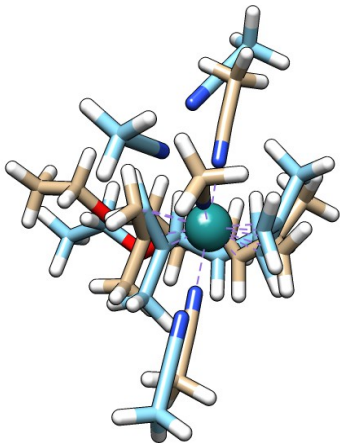

Figure 42: Molecular structure with the **HAYKIC** CSD code. Example of the **G.2** fragment. Colour code: X-ray structure carbon atoms (brown) ReaxFF-energy-minimized-structure carbon atoms (light blue) nitrogen atoms (blue) oxygen atoms (red)

6 Discussion of the coordinate and the interatomic distances approach

Early in the evaluation of the force field, the WRMSD distribution (**Figure 6**), the MUE and MSE of all distances (**Figure 9**), and of individual molecules (**Figure 10**). Showed a clear overestimation in ruthenium-nitrogen bond length. In some of these overestimations is clear the dissociation of the bond (e.g. nitro, and acetonitrile ligands in **Figure 41** and **Figure 42**).

The ratio of the different atoms showed a lack of correlation, between these and the MUE, MSE values. Meaning that the number of certain atom/atoms within a molecule were not related with the longest overestimations. This supports the idea, that the longest overestimations found along the study, were isolated cases that depend in the chemical environment (neighbouring atoms or ligands).

To complement the ratio study, the $e_{C\text{-}N}$, and $e_{Ru\text{-}O}$ were plotted against the number of ruthenium-nitrogen and ruthenium-oxygen bonds respectively, two facts were observed: (1) the longest overestimations in the C-N bond length were not related with the number of Ru-N bonds (**Figure 16**). (2) the $e_{Ru\text{-}O}$ decrease in relative values, to values close to zero, when the number of Ru-O bonds were increased within a molecule (**Figure 17**). This second fact is probably related with the molecules used in the training set, where ruthenium chemical structures, from surfaces interacting with oxygen, carbon and hydrogen atoms or simple molecules (containing these atoms) were used to train and parametrize ReaxFF.

Later in the study, the sorted $e_{C\text{-}C}$, $e_{C\text{-}N}$, $e_{C\text{-}O}$, $e_{N\text{-}O}$, $e_{Ru\text{-}C}$, $e_{Ru\text{-}O}$ and $e_{Ru\text{-}N}$ pointed the longest overestimations. Where in most of the cases, there is a ruthenium-nitrogen interaction close to the interatomic distance under study.

The $e_{C\text{-}N}$ longest overestimation showed a bond breaking in an azo-ligand (**Figure 11**), where the C-N bond distance was overestimated from **1.39 Å** to **2.41Å**. In the case of triazole ligands, the C-N reference distances within the heteroaromatic system (**A.2** in **Figure 19**) were overestimated (e.g. from **1.37 Å** to **2.137 Å**). The diazole ligands $e_{C\text{-}N}$ (**A.3** in **Figure 19**) where ruthenium atom was bonded to nitrogen were overestimated (e. g. from **1.35 Å** to **1.97 Å**). The same ligands with carbon atom bonded to ruthenium were below these overestimations (e.g. from **1.39Å** to **1.78 Å**).

The $e_{C\text{-}O}$ longest overestimations were found close to a ruthenium-nitrogen bond (e.g. **B.1**, **B.2** and **B.3** in **Figure 22**). These C-O bond lengths were overestimated from **1.31 Å**, **1.21 Å**, **1.31 Å** to **2.33 Å**, **2.152 Å**, and **2.13 Å** respectively. The sorted $e_{C\text{-}O}$ reflected a good estimation in C-O triple bonds from carbonyl ligands, followed by C-O double bonds from ketones and single bonds from OH groups (**B.7**,

B.8 and **B.9** in **Figure 22**).

The most substantial deviations in the calculation of the C-C bond lengths were found between nitrogens: (1) from cyclic imines where the bond was broken, an overestimation from **1.44 Å** to **3.02 Å**, was observed (**C.1** in **Figure 26**) (2) secondary and tertiary amines (**C.4**, **C.5** in **Figure 26**) were overestimated from **1.49 Å**, **1.5 Å** to **2.37 Å**, **2.21 Å** respectively. Also $e_{C\text{-}C}$ from carbons in pyridine system and carbonyl groups were found (**C.3** in **Figure 26**). These bonds were overestimated from **1.49Å** to **2.11 Å**.

Some deviations in the N-O bond lengths were found in nitro groups and had the largest overestimations from **1.19 Å** to **1.63 Å**. The largest underestimation from **2.35 Å** to **1.62 Å** was found in a heterocyclic compound (**F.8** in **Figure 38**).

The largest deviations for Ru-C bond lengths were associated with Ru-aromatic interactions (**E.1** in **Figure 35**) where the maximum overestimations were found from **2.20Å** to **3.94 Å**.

The $e_{Ru\text{-}N}$ reflected an obvious need for parametrising ruthenium-nitrogen interactions, most of the bonds were dissociated (from **1.84 Å** to **3.82 Å**).

Figure 43 shows the longest overestimations for each interaction. This can suggest structures that can be chosen for parametrising ReaxFF and expand substantially the fields of application.

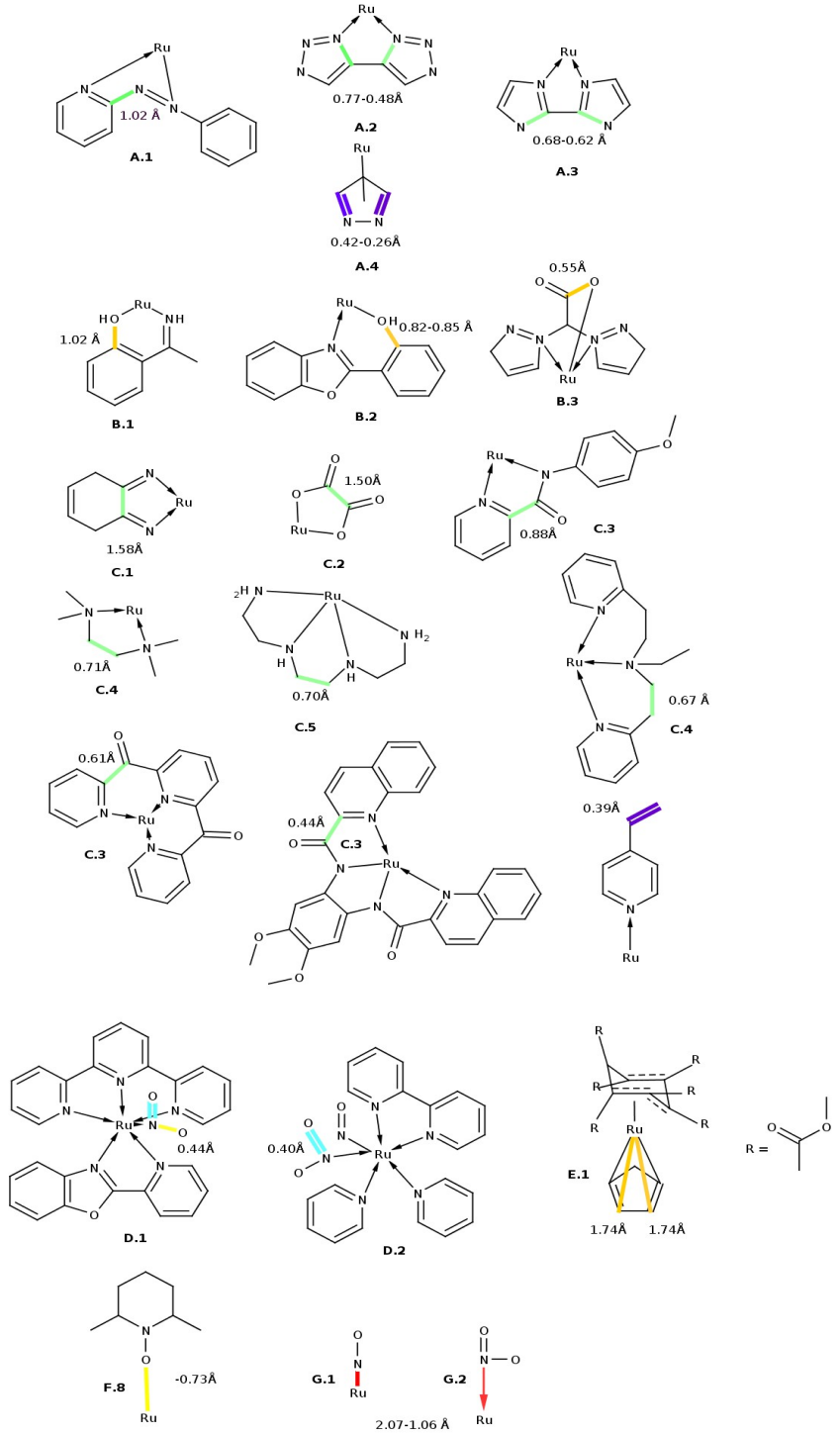

Figure 43: Largest overestimations of every interaction

7 Conclusion

The largest bond overestimations in ReaxFF-minimized-structures were found in Ru-N bonds, wherein some of the cases the bond length was larger than the sum of the van der Waals radii of Ru and N. There also seems to be an influence of Ru-N bonds in the largest overestimations of the other bond lengths included in this study. Some of these bonds were broken or had a considerably long bond distance. Nevertheless, there does not seem to be a relation between the number of ruthenium-nitrogen bonds and the longest overestimations of bond lengths. Not correlation of the fraction of different kind of atoms with the MUE or the MSE was found either.

The fact that ReaxFF overestimates considerably the C-N distances between the imidazol ring suggests that this method will present low accuracy in the study of olefin metathesis reactions. Nonetheless a possibility to carry out this kind of studies would be to freeze those C-N interactions. A more desirable alternative, would be to parametrize the force field, including diazole and triazole ligands.

In the case of Ruthenium-olefin interactions, even if the analysis does not show any big overestimation, within these type of compounds, a deeper analysis should be made.

(1) Seddon, E. A.; Seddon K. R. *The Chemistry of Ruthenium*; Elsevier: Amsterdam, 1984.
(2) Griffith, W. P. *The Chemistry of the Rarer Platinum Metals: Os, Ru, Ir and Rh*; Wiley Interscience: New York, 1967.
(3) Cotton, F. A.; Willkinson. G. *Advanced Inorganic Chemistry*; 4th ed.; John Wiley & Sons: New York, 1980.
(4) Lee, D. G.; van den Engh, M. *Oxidation in Organic Chemistry*; Academic Press.; New York, 1973.
(5) J. L. Courtney. *Organic Synthesis by Oxydation with Metal Compounds*; Mijs W. J. de Jonge, C. R. H. I.; Plenum Press: New York, 1986.
(6) Paquette, L.A., S., S. Encyclopedia of Reagents for Organic Synthesis. In; Chichester, 1996; Vol. 6, p. 4410.
(7) Bennet, M. A.; Matheson, T. W. *Comprehensive Organometallic Chemistry*; Wilkinson, G., Stone, F. G. A., Abel, E. W.; Pergamon Press: Oxford, 1982.
(8) James B. R. *Homogeneus Hydrogenation*; Wiley: 1973, New York.
(9) Freifelder, M. *Practical Catalytic Hydrogenation*; Wiley-Interscience.; New York, 1971.
(10) Komiya, S.; Hirano, M. Synthesis of Organometallic Compounds. In; Chichester, 1997; p. 159.
(11) Gessler, S.; Randl, S.; Blechert, S. Synthesis and Metathesis Reactions of a Phosphine-Free Dihydroimidazole Carbene Ruthenium Complex. *Tetrahedron Lett.* **2000**, *41*, 9973–9976.
(12) Herrmann, W. A. N-Heterocyclic Carbenes: A New Concept in Organometallic Catalysis. *Angew. Chem. Int. Ed.* **2002**, *41*, 1290–1309.
(13) Trost, B. M. The Atom Economy - a Search for Synthetic Efficiency. **1991**, 1471–1478.
(14) Grubbs, R. H. *Handbook of Metathesis*; Wiley-VCH.; Weinheim, 2003.
(15) Scholl, M.; Ding, S.; Lee, C. W.; Grubbs, R. H. Synthesis and Activity of a New Generation of Ruthenium-Based Olefin Metathesis Catalysts Coordinated with 1,3-Dimesityl-4,5-Dihydroimidazol-2-Ylidene Ligands§. *Org. Lett.* **1999**, *1*, 953–956.
(16) Weskamp, T.; Schattenmann, W. C.; Spiegler, M.; Herrmann, W. A. A Novel Class of Ruthenium Catalysts for Olefin Metathesis. *Angew. Chem. Int. Ed.* **1998**, *37*, 2490–2493.
(17) Huang, J.; Stevens, E. D.; Nolan, S. P.; Petersen, J. L. Olefin Metathesis-Active Ruthenium Complexes Bearing a Nucleophilic Carbene Ligand. *J. Am. Chem. Soc.* **1999**, *121*, 2674–2678.
(18) Halbach, T. S.; Mix, S.; Fischer, D.; Maechling, S.; Krause, J. O.; Sievers, C.; Blechert, S.; Nuyken, O.; Buchmeiser, M. R. Novel Ruthenium-Based Metathesis Catalysts Containing Electron- Withdrawing Ligands: Synthesis, Immobilization, and Reactivity. *J. Org. Chem.* **2005**, *70*, 4687–4694.
(19) Garber, S. B.; Kingsbury, J. S.; Gray, B. L.; Hoveyda, A. H. Efficient and Recyclable Monomeric and Dendritic Ru-Based Metathesis Catalysts. *J. Am. Chem. Soc.* **2000**, *122*, 8168–8179.
(20) Occhipinti, G.; Hansen, F. R.; Törnroos, K. W.; Jensen, V. R. Simple and Highly Z-Selective Ruthenium-Based Olefin Metathesis Catalyst. *J. Am. Chem. Soc.* **2013**, *135*, 3331–3334.
(21) Sanford, M. S.; Ulman, M.; Grubbs, R. H. New Insights into the Mechanism of Ruthenium-Catalyzed Olefin Metathesis Reactions. *J. Am. Chem. Soc.* **2001**, *123*, 749–750.
(22) Sanford, M. S.; Love, J. A.; Grubbs, R. H. Mechanism and Activity of Ruthenium Olefin Metathesis Catalysts. *J. Am. Chem. Soc.* **2001**, *123*, 6543–6554.
(23) Basu, K.; Cabral, J. A.; Paquette, L. A. Comparative Investigation of Kinetic Consequences Associated with Long-Range Electronic Effects on Catalytic Ruthenium-Promoted Ring-Closing Metathesis. *Tetrahedron Lett.* **2002**, *43*, 5453–5456.
(24) Lehman, S. E.; Wagener, K. B. Comparison of the Kinetics of Acyclic Diene Metathesis Promoted by Grubbs Ruthenium Olefin Metathesis Catalysts. *Macromolecules* **2002**, *35*, 48–53.
(25) Adlhart, C.; Chen, P. Mechanism and Activity of Ruthenium Olefin Metathesis Catalysts: The

Role of Ligands and Substrates from a Theoretical Perspective. *J. Am. Chem. Soc.* **2004**, *126*, 3496–3510.
(26) Torker, S.; Merki, D.; Chen, P. Gas-Phase Thermochemistry of Ruthenium Carbene Metathesis Catalysts. *J. Am. Chem. Soc.* **2008**, *130*, 4808–4814.
(27) Hejl, A.; Day, M. W.; Grubbs, R. H. Latent Olefin Metathesis Catalysts Featuring Chelating Alkylidenes. *Organometallics* **2006**, *25*, 6149–6154.
(28) Clavier, H.; Nolan, S. P. N-Heterocyclic Carbene and Phosphine Ruthenium Indenylidene Precatalysts: A Comparative Study in Olefin Metathesis. *Chem. – Eur. J.* **2007**, *13*, 8029–8036.
(29) Da Costa, R. C.; Gladysz, J. A. Syntheses and Reactivity of Analogues of Grubbs' Second Generation Metathesis Catalyst with Fluorous Phosphines: A New Phase-Transfer Strategy for Catalyst Activation. *Adv. Synth. Catal.* **2007**, *349*, 243–254.
(30) Hong, S. H.; Wenzel, A. G.; Salguero, T. T.; Day, M. W.; Grubbs, R. H. Decomposition of Ruthenium Olefin Metathesis Catalysts. *J. Am. Chem. Soc.* **2007**, *129*, 7961–7968.
(31) Bieniek, M.; Michrowska, A.; Usanov, D. L.; Grela, K. In an Attempt to Provide a User's Guide to the Galaxy of Benzylidene, Alkoxybenzylidene, and Indenylidene Ruthenium Olefin Metathesis Catalysts. *Chem. – Eur. J.* **2008**, *14*, 806–818.
(32) Clavier, H.; Urbina-Blanco, C. A.; Nolan, S. P. Indenylidene Ruthenium Complex Bearing a Sterically Demanding NHC Ligand: An Efficient Catalyst for Olefin Metathesis at Room Temperature. *Organometallics* **2009**, *28*, 2848–2854.
(33) Jarzembska, K.; Seal, S.; Woźniak, K.; Szadkowska, A.; Bieniek, M.; Grela, K. X-Ray Photoelectron Spectroscopy and Reactivity Studies of a Series of Ruthenium Catalysts. *ChemCatChem* **2009**, *1*, 144–151.
(34) Broggi, J.; Urbina-Blanco, C. A.; Clavier, H.; Leitgeb, A.; Slugovc, C.; Slawin, A. M. Z.; Nolan, S. P. The Influence of Phosphane Ligands on the Versatility of Ruthenium–Indenylidene Complexes in Metathesis. *Chem. – Eur. J.* **2010**, *16*, 9215–9225.
(35) Eide, E. F. van der; Piers, W. E. Mechanistic Insights into the Ruthenium-Catalysed Diene Ring-Closing Metathesis Reaction. *Nat. Chem.* **2010**, *2*, 571–576.
(36) Keitz, B. K.; Grubbs, R. H. Probing the Origin of Degenerate Metathesis Selectivity via Characterization and Dynamics of Ruthenacyclobutanes Containing Variable NHCs. *J. Am. Chem. Soc.* **2011**, *133*, 16277–16284.
(37) Xi, Z.; Bazzi, H. S.; Gladysz, J. A. Analogs of Grubbs' Second Generation Catalyst with Hydrophilic Phosphine Ligands: Phase Transfer Activation of Ring Closing Alkene Metathesis. *Org. Lett.* **2011**, *13*, 6188–6191.
(38) Thiel, V.; Hendann, M.; Wannowius, K.-J.; Plenio, H. On the Mechanism of the Initiation Reaction in Grubbs–Hoveyda Complexes. *J. Am. Chem. Soc.* **2012**, *134*, 1104–1114.
(39) Vyboishchikov, S. F.; Bühl, M.; Thiel, W. Mechanism of Olefin Metathesis with Catalysis by Ruthenium Carbene Complexes: Density Functional Studies on Model Systems. *Chem. – Eur. J.* **2002**, *8*, 3962–3975.
(40) Adlhart, C.; Chen, P. Ligand Rotation Distinguishes First- and Second-Generation Ruthenium Metathesis Catalysts. *Angew. Chem. Int. Ed Engl.* **2002**, *41*, 4484–4487.
(41) Fomine, S.; Vargas, S. M.; Tlenkopatchev, M. A. Molecular Modeling of Ruthenium Alkylidene Mediated Olefin Metathesis Reactions. DFT Study of Reaction Pathways. *Organometallics* **2003**, *22*, 93–99.
(42) Bernardi, F.; Bottoni, A.; Miscione, G. P. DFT Study of the Olefin Metathesis Catalyzed by Ruthenium Complexes. *Organometallics* **2003**, *22*, 940–947.
(43) Cavallo, L. Mechanism of Ruthenium-Catalyzed Olefin Metathesis Reactions from a Theoretical Perspective. *J. Am. Chem. Soc.* **2002**, *124*, 8965–8973.

(44) Costabile, C.; Cavallo, L. Origin of Enantioselectivity in the Asymmetric Ru-Catalyzed Metathesis of Olefins. *J. Am. Chem. Soc.* **2004**, *126*, 9592–9600.
(45) Vyboishchikov, S. F.; Thiel, W. Ring-Closing Olefin Metathesis on Ruthenium Carbene Complexes: Model DFT Study of Stereochemistry. *Chem. – Eur. J.* **2005**, *11*, 3921–3935.
(46) Fomine, S.; Ortega, J. V.; Tlenkopatchev, M. A. Computational Modeling of Ruthenium Alkylidene Mediated Olefin Metathesis: A DFT Study of Reaction Pathways for the Ring-Opening Cross-Metathesis of Norbornene with Olefins. *J. Mol. Catal. Chem.* **2005**, *236*, 156–161.
(47) Lippstreu, J. J.; Straub, B. F. Mechanism of Enyne Metathesis Catalyzed by Grubbs Ruthenium−Carbene Complexes: A DFT Study. *J. Am. Chem. Soc.* **2005**, *127*, 7444–7457.
(48) Tsipis, A. C.; Orpen, A. G.; Harvey, J. N. Substituent Effects and the Mechanism of Alkene Metathesis Catalyzed by Ruthenium Dichloride Catalysts. *Dalton Trans.* **2005**, 2849–2858.
(49) Zhao, Y.; Truhlar, D. G. Density Functionals with Broad Applicability in Chemistry. *Acc. Chem. Res.* **2008**, *41*, 157–167.
(50) Zhao, Y.; Truhlar, D. G. Attractive Noncovalent Interactions in the Mechanism of Grubbs Second-Generation Ru Catalysts for Olefin Metathesis. *Org. Lett.* **2007**, *9*, 1967–1970.
(51) Diesendruck, C. E.; Tzur, E.; Ben-Asuly, A.; Goldberg, I.; Straub, B. F.; Lemcoff, N. G. Predicting the Cis−Trans Dichloro Configuration of Group 15−16 Chelated Ruthenium Olefin Metathesis Complexes: A DFT and Experimental Study. *Inorg. Chem.* **2009**, *48*, 10819–10825.
(52) Fomine, S.; Tlenkopatchev, M. A. Ring-Opening of Cyclohexene via Metathesis by Ruthenium Carbene Complexes. A Computational Study. *Organometallics* **2007**, *26*, 4491–4497.
(53) Fomine, S.; Ortega, J. V.; Tlenkopatchev, M. A. Metathesis of Halogenated Olefins: A Computational Study of Ruthenium Alkylidene Mediated Reaction Pathways. *J. Mol. Catal. Chem.* **2007**, *263*, 121–127.
(54) Fomine, S.; Tlenkopatchev, M. A. Cross-Metathesis of Dimethyl Maleate and Ethylene Catalyzed by Second Generation Ruthenium Carbene Complexes: B3LYP and MPW1K Comparison Study. *J. Organomet. Chem.* **2006**, *691*, 5189–5196.
(55) Tonner, R.; Frenking, G. Are Carbodiphosphoranes Better Ligands than N-Heterocyclic Carbenes for Grubb's Catalysts? *Chem. Commun.* **2008**, 1584–1586.
(56) Poater, A.; Ragone, F.; Correa, A.; Szadkowska, A.; Barbasiewicz, M.; Grela, K.; Cavallo, L. Mechanistic Insights into the Cis–trans Isomerization of Ruthenium Complexes Relevant to Catalysis of Olefin Metathesis. *Chem. – Eur. J.* **2010**, *16*, 14354–14364.
(57) Zhao, Y.; Truhlar, D. G. Applications and Validations of the Minnesota Density Functionals. *Chem. Phys. Lett.* **2011**, *502*, 1–13.
(58) Costabile, C.; Mariconda, A.; Cavallo, L.; Longo, P.; Bertolasi, V.; Ragone, F.; Grisi, F. The Pivotal Role of Symmetry in the Ruthenium-Catalyzed Ring-Closing Metathesis of Olefins. *Chem. – Eur. J.* **2011**, *17*, 8618–8629.
(59) Yang, H.-C.; Huang, Y.-C.; Lan, Y.-K.; Luh, T.-Y.; Zhao, Y.; Truhlar, D. G. Carbene Rotamer Switching Explains the Reverse Trans Effect in Forming the Grubbs Second-Generation Olefin Metathesis Catalyst. *Organometallics* **2011**, *30*, 4196–4200.
(60) Occhipinti, G.; Jensen, V. R. Nature of the Transition Metal–Carbene Bond in Grubbs Olefin Metathesis Catalysts. *Organometallics* **2011**, *30*, 3522–3529.
(61) Minenkov, Y.; Singstad, Å.; Occhipinti, G.; Jensen, V. R. The Accuracy of DFT-Optimized Geometries of Functional Transition Metal Compounds: A Validation Study of Catalysts for Olefin Metathesis and Other Reactions in the Homogeneous Phase. *Dalton Trans.* **2012**, *41*, 5526–5541.
(62) Occhipinti, G.; Bjørsvik, H.-R.; Jensen, V. R. Quantitative Structure−Activity Relationships of

Ruthenium Catalysts for Olefin Metathesis. *J. Am. Chem. Soc.* **2006**, *128*, 6952–6964.
(63) Minenkov, Y.; Occhipinti, G.; Jensen, V. R. Complete Reaction Pathway of Ruthenium-Catalyzed Olefin Metathesis of Ethyl Vinyl Ether: Kinetics and Mechanistic Insight from DFT. *Organometallics* **2013**, *32*, 2099–2111.
(64) Van Duin, A. C. T.; Dasgupta, S.; Lorant, F.; Goddard, W. A. ReaxFF: A Reactive Force Field for Hydrocarbons. *J. Phys. Chem. A* **2001**, *105*, 9396–9409.
(65) Gabriel Cuevas; Fernando Cortés. *Introducción a La Química Computacional*; Primera edición.; Fondo de cultura económica: México, 2003.
(66) Landis, C. R.; Lipkowits, K. B.; Boyd, D. B. Reviews in Computational Chemistry. In; 6 VCH; 1955.
(67) Allinger, L.; Burket, U. Molecular Mechanics. *ACS Monogr.* **1982**, *177*, 184–189.
(68) Allinger, N. L.; Yan, J. J. Am. Chem. Soc. **1993**, *115*, 11918.
(69) Nevins, N., J. J. Comput. Chem. **1996**, *17*, 669, 695, 730.
(70) Cornell W. D. J. Am. Chem. Soc. **1995**, *117*, 5179.
(71) Weineret, S. J. J. Comput. Chem. **1986**, *7*, 230.
(72) Weiner, S. J. J. Am. Chem. Soc. **1984**, *106*, 765.
(73) Brooks, B. R. J. Comput. Chem. **1993**, *4*, 187.
(74) Mackerell, A. D. J. Am. Chem. Soc. **1995**, *117*, 11946.
(75) Jorgensen, W. L.; Tirado-Rives, J. J. Am. Chem. Soc. **1988**, *110*, 1657.
(76) Halgren, T. A. J. Comput. Chem. **1996**, *17*, 490, 553, 616.
(77) Hwang, M. J.; Stockfish, T. P.; Hagler, A. T. J. Am. Chem. Soc. **1994**, *116*, 2515.
(78) Zimmer, M. Chem. Rev. **1995**, *95*, 2629.
(79) Stuart, S. J.; Tutein, A. B.; Harrison, J. A. J. Chem. Phys. **2000**, *112*, 6472–6486.
(80) Brenner, D. W. Empirical Potential for Hydrocarbons for Use in Simulating the Chemical Vapor Deposition of Diamond Films. *Phys. Rev. B* **1990**, *42*, 9458–9471.
(81) Polzer, T.; Kiefer, W. General Valence Force Fields of the Free and the Coordinated Cyclopentadienyl Anion. *J. Organomet. Chem.* **1996**, *508*, 153–157.
(82) Tersoff, J. New Empirical Approach for the Structure and Energy of Covalent Systems. *Phys. Rev. B* **1988**, *37*, 6991–7000.
(83) Chenoweth, K.; van Duin, A. C. T.; Goddard, W. A. ReaxFF Reactive Force Field for Molecular Dynamics Simulations of Hydrocarbon Oxidation. *J. Phys. Chem. A* **2008**, *112*, 1040–1053.
(84) Iii, W. A. G.; Duin, A. van; Chenoweth, K.; Cheng, M.-J.; Pudar, S.; Oxgaard, J.; Merinov, B.; Jang, Y. H.; Persson, P. Development of the ReaxFF Reactive Force Field for Mechanistic Studies of Catalytic Selective Oxidation Processes on BiMoO X. *Top. Catal.* **2006**, *38*, 93–103.
(85) Goddard, W.; Merinov, B.; van Duin, A.; Jacob, T.; Blanco, M.; Molinero, V.; Jang, S. S.; Jang, Y. H. Multi-Paradigm Multi-Scale Simulations for Fuel Cell Catalysts and Membranes. *Mol. Simul.* **2006**, *32*, 251–268.
(86) Nielson, K. D.; van Duin, A. C. T.; Oxgaard, J.; Deng, W.-Q.; Goddard, W. A. Development of the ReaxFF Reactive Force Field for Describing Transition Metal Catalyzed Reactions, with Application to the Initial Stages of the Catalytic Formation of Carbon Nanotubes. *J. Phys. Chem. A* **2005**, *109*, 493–499.
(87) Chen, N.; Lusk, M. T.; van Duin, A. C. T.; Goddard, W. A. Mechanical Properties of Connected Carbon Nanorings via Molecular Dynamics Simulation. *Phys. Rev. B* **2005**, *72*, 085416.
(88) Che, J.; Çagin, T.; Iii, W. A. G. Studies of Fullerenes and Carbon Nanotubes by an Extended Bond Order Potential. *Nanotechnology* **1999**, *10*, 263.
(89) Johnston, H. S.; Parr, C. Activation Energies from Bond Energies. I. Hydrogen Transfer Reactions. *J. Am. Chem. Soc.* **1963**, *85*, 2544–2551.

(90) Cleveland, T.; Landis, C. R. Valence Bond Concepts Applied to the Molecular Mechanics Description of Molecular Shapes. 2. Applications to Hypervalent Molecules of the P-Block. *J. Am. Chem. Soc.* **1996**, *118*, 6020–6030.
(91) Mortier, W. J.; Ghosh, S. K.; Shankar, S. Electronegativity-Equalization Method for the Calculation of Atomic Charges in Molecules. *J. Am. Chem. Soc.* **1986**, *108*, 4315–4320.
(92) Rappe, A. K.; Goddard, W. A. Charge Equilibration for Molecular Dynamics Simulations. *J. Phys. Chem.* **1991**, *95*, 3358–3363.
(93) Chenoweth, K.; Cheung, S.; van Duin, A. C. T.; Goddard, W. A.; Kober, E. M. Simulations on the Thermal Decomposition of a Poly(dimethylsiloxane) Polymer Using the ReaxFF Reactive Force Field. *J. Am. Chem. Soc.* **2005**, *127*, 7192–7202.
(94) Maurice G. Kendall; William R. Buckland. *Dictionary of Statistical Terms*; Edinburgh, 1960.
(95) Allen, F. H. *The Cambridge Structural Database: A Quarter of Million Crystal Structures and Rising*; 2002.
(96) Bruno, J.; Cole, J. C.; Edgington, P. R.; Kessler, M.; Macrae, C. F.; McCabe, P.; Pearson, J.; Taylor, R. New Software for Searching the Cambridge Structural Database and Visualising Crystal Structures. *Acta Crystallogr B58* **2002**, 389–397.
(97) Foscato, M.; Occhipinti, G.; Venkatraman, V.; Alsberg, B. K.; Jensen, V. R. Automated Design of Realistic Organometallic Molecules from Fragments. *J. Chem. Inf. Model.* **2014**.
(98) Dang, Y.; Wang, Z.-X.; Wang, X. A Thorough DFT Study of the Mechanism of Homodimerization of Terminal Olefins through Metathesis with a Chelated Ruthenium Catalyst: From Initiation to Z Selectivity to Regeneration. *Organometallics* **2012**, *31*, 7222–7234.
(99) David J. Heisterberg. *Quatfit*; 1990.

11 DFT-structures included in the dataset

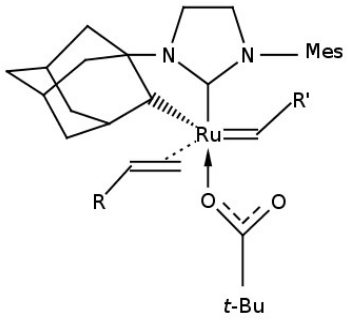

1

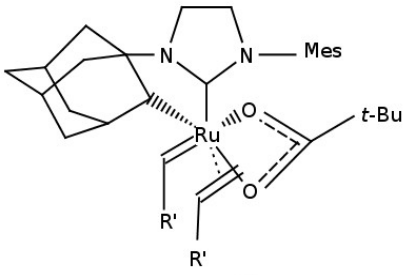

2

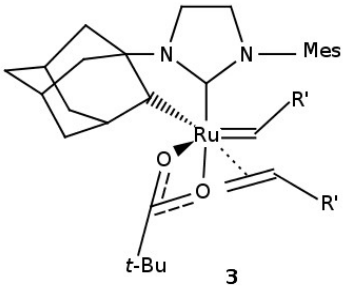

3

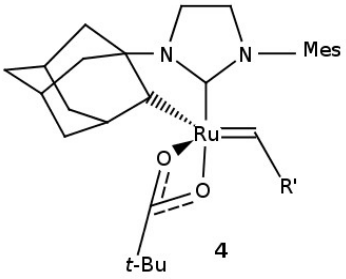

4

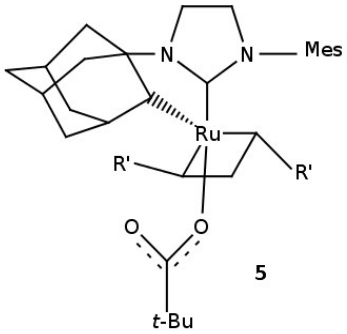

5

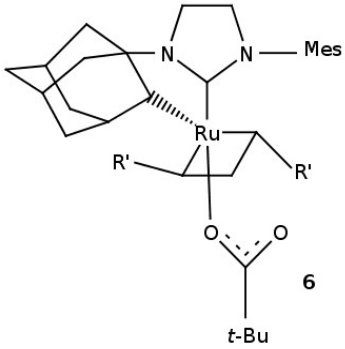

6

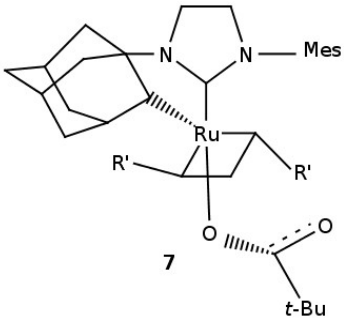

7

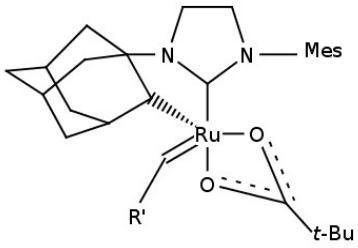

8

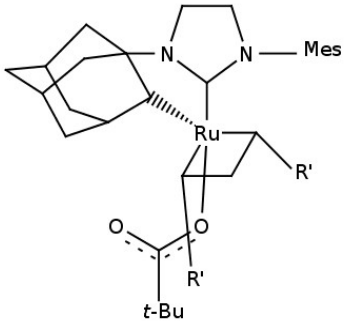

9

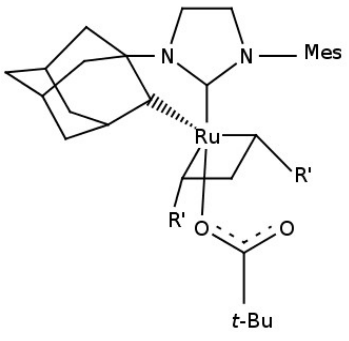

10

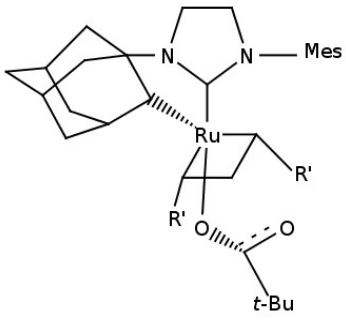

11

A List of the code of 786 X-ray structures from the CSD included in the dataset

1	BAWPUM	28	DUMGEY	59	ESIXEK
2	AFODIJ	29	DUXCII	60	ETOXIU
3	DAFXAL	30	EBAFOE	61	EYIZUI
4	DAMBEA	31	EBAHAS	62	EZIYAN
5	DAMBIE	32	EBEDUK	63	FAHVUG
6	DAMCAX	33	EBILUW	64	FAHYOE
7	DAQGUY	34	EBIMAD	65	FAHYUK
8	DATHIP01	35	AGASUW	66	FAJREP
9	DATHIP13	36	EBIMEH	67	FAJXIY
10	DAZFIT	37	ECOQUJ	68	ALEJAC
11	DEKSOC	38	EFOFEK	69	FAKMOT
12	DEXFAO	39	EFUSIH	70	FANDAA
13	AFODOP	40	EFUSIH01	71	FANPER
14	DEYDIV	41	EJIGEK	72	FANPIV
15	DEYPAY	42	EJIROE	73	FANQIW
16	DIFJUY	43	ELANUB	74	FECCAT
17	DIJPUI	44	ELAPAJ	75	FEFVAN
18	DOCCON	45	ELAPEN	76	FEPQOH
19	DOHGEN	46	AHIHII	77	FEPXII
20	DOHSUP	47	ELETIY	78	FEPXOO
21	DOHSUP01	48	ELETOE	79	ALEROY
22	DOHSUP02	49	ELETUK	80	FEVMOI
23	DOPDIV	50	ENACEB	81	FEYMOL
24	AGASOQ	51	ENAVUL	82	FEYMOL10
25	DOTBEU	52	EQOZAM	83	FEZSIN
26	DOZQIS	53	ERAYUR	84	FIHQUI
27	DUDLUK	54	EREDIO	85	FOPRIM
		55	EREDOU	86	FORQOS
		56	ESEBUZ	87	FUBPEX
		57	AHUSOL	88	FUGMEA
		58	ESILEX	89	FUJZAL

90	AMAPAG	121	HAHSIS	152	HOMCAN
91	FUJZAL01	122	HAKDAZ	153	HOMKUQ
92	FULRIO	123	HANYIE	154	HONHOI
93	FUNPOU	124	ASELIU	155	HOWKUA
94	FURTER	125	HANYOK	156	HOWSOB
95	FUTROC	126	HARHEN	157	AVIBAJ
96	FUTRUI	127	HASSEZ	158	HOWSUH
97	FUVDAC	128	HATNUN	159	HOWTAO
98	GABREI	129	HATPAV	160	HOWTES
99	GACMAA	130	HATPEZ	161	HOZKIR
100	GAJXEU	131	HAYKIC	162	HUHMUT
101	AQIHEO	132	HBRUCO10	163	HUNSAL
102	GAVQIF	133	HEDDUQ	164	HUNSIT
103	GAWTED	134	HEGMIP	165	HUQPIT
104	GAWTED01	135	ATIJAO	166	HUWLUH
105	GAZSAB	136	HEGMIP01	167	HUXQIA
106	GEMWEA	137	HEHPUF	168	AXIVAE
107	GEMWOK	138	HELRUL	169	HVIORU
108	GERMAR	139	HETZAH	170	HXDPRU10
109	GIMWAA	140	HEYXEO	171	IBAWOZ
110	GINSUR	141	HEYXIS	172	ICIVIZ
111	GITMUR	142	HIFLIS	173	ICOPAT
112	BAWQAT	143	HIRFAP01	174	ICOPOH
113	ARIPIA	144	HIVDIA	175	IDAKAB
114	GOCMOB	145	HIVVEN	176	IDAKEF
115	GONRIK	146	ATOVOV	177	IDAVEQ
116	GONROQ	147	HIVVUD	178	IDONAR
117	GOZYOJ	148	HIZSIT	179	AYITOS
118	GUQQOZ	149	HMBZRU10	180	IFAXUI
119	HABHUP	150	HOBSAT	181	IFAYAP
120	HABJAX	151	HOLXAH	182	IFAYIX

183 IFEVAR
184 IFEYUN
185 IFEZAU
186 IFEZEY
187 IHEQAO
188 IHEXOI
189 IHIVOK
190 BAFKUP
191 IKENAN
192 IKOFOE
193 IKOGEV
194 ILUSIR
195 ILUZAR
196 IMIDEO
197 IMOXIR
198 IPEQUP
199 IPERAW
200 IPEREA
201 BAFLAW
202 IQIQOP
203 IQIQUV
204 IREGUI
205 ISEVAE
206 ISUKIR
207 IXEMIH
208 IXEMIH01
209 IXOQAO
210 IXOQES
211 IYOKEM
212 BAFLIE
213 IZATIN
214 IZUMIA
215 IZUXOR
216 JAHFUU
217 JAJMIQ
218 JASFOY
219 JEDGOO
220 JEDNEM
221 JEFDII
222 JEMBOS
223 FAVWIK
224 BAFLOK
225 JENCAH
226 JENGAL
227 JISVIR
228 JITYIV
229 JIWDOI
230 JIYSEQ
231 JIYSIU
232 JIYSOA
233 JIYTER
234 JIYTIV
235 BAFMAX
236 JODLIX
237 JOFYIN
238 JOJQUV
239 JOLYOY
240 JOQRUC
241 JOSRIS
242 JOZJIR
243 JUMXOE
244 JURMAK
245 KABVEQ
246 BAQLAI
247 KAJHAF
248 KAJHEJ
249 KAJHUZ
250 KAQDUD
251 KARTEC
252 KARVUV
253 KASMIC
254 KASMOI
255 KASNEZ
256 KAWMUQ
257 BAQTES
258 KAWQEE
259 KAZJOL
260 KECZUN
261 KELLIW
262 KEMTUR
263 KEMTUR01
264 KEWQOT
265 KIRQEH
266 KIVPEL
267 KIVPIP
268 BAWPEU
269 KIVROW
270 KIWRUD
271 KIZSAN
272 KIZSIW
273 KIZSUI
274 KIZTOD
275 KOFWOS

276 KOKWOW
277 KOLRIM
278 KOZRIA
279 BAXZOP
280 KUCJOH
281 KUCJUN
282 KUFDOE
283 KUGPEI
284 KUVMAP
285 KUVMET
286 LAHQER
287 LAHQIV
288 LATVIM
289 LEGZEC01
290 BAYBEI
291 LELREA
292 LETSEJ
293 LICQIY
294 LIFDAF
295 LIMSUV
296 LIPNAZ
297 LIPNED
298 LIQYAM
299 LIYPEP
300 LIYPIT
301 BAZMAQ
302 LIZFOP
303 LOCRIE
304 LONYIX
305 LOQPAJ
306 LOTVAR
307 LUKPEN
308 LULBOJ
309 LUNFEG
310 LUQNEQ
311 LUQNEQ01
312 BDMFRU
313 LUQYOM
314 LURFEJ
315 LUWJET
316 LUWLAR
317 LUWLEV
318 MABWIW
319 MABXIX
320 MADTOB
321 MAFHUX
322 MAHVAS
323 BEBQAA
324 MAJJAK
325 MAQQAW
326 MAQQEA
327 MARBUC
328 MARCEN
329 MARVEH
330 MARYAG
331 MARYEK
332 MAWVAH
333 MAWVAH01
334 NECJOW
335 BECMAX
336 MEBTAO
337 MEBTES
338 MEJBIM
339 MEMGEQ
340 MEMJOE
341 MESFAS
342 MESFEW
343 MIDMAO
344 MILXOU
345 MILXUA
346 BECMEB
347 MILYAH
348 MIMSUW
349 MIVKEI
350 MIXJOT
351 MIYNEO
352 MIZSOE
353 MOCPRU
354 MOCPRU10
355 MOGRIK
356 MOMWUG
357 BECMUR
358 MOMXAN
359 MOMXER
360 MOXNET
361 MUDKIG
362 MUGJUU
363 MUGMIL
364 MUGMOR
365 MUNFIK
366 MUNWAU
367 MUPBUU
368 BEGCEW

369 MUZSEF
370 MUZSIJ
371 NABXOE
372 NABYAR
373 NADPUD
374 NAFJAF
375 NAGDOP
376 NAHNAN
377 NAHNER
378 NAJXUS
379 BEYQAY
380 NAPYUZ
381 NAPZEK
382 NAPZOU
383 NAQSII
384 NAQTAB
385 NAQTEF
386 NAQTIJ
387 NAWJEB
388 NEFXUS01
389 NEFXUS02
390 BIBYOA
391 NEHBUY
392 NEHCAF
393 NEHLER
394 NETMUV
395 NETNAC
396 NIFMUK
397 NIFNAR
398 NIFNEV
399 NIPHIE
400 NIQRIO
401 BIGBID
402 NODZEM
403 NODZIQ
404 NOFPII
405 NOGRIK
406 NONLIM
407 NUCFOH
408 OBEYIE
409 OCEPUH
410 ODICIP
411 OGEXON
412 BIMFIN
413 OHOZAM
414 OHUSEP
415 OJELEV
416 OJELIZ
417 OJELOF
418 OJELUL
419 ONAJIX
420 ORALEZ
421 OSULOE
422 OWALUU
423 BIQMAP
424 OWUKEX
425 PALLEU
426 PALLIY
427 PAQTIK
428 PAXFAW
429 PAYXET
430 PAYXIX
431 PAYXOD
432 PAYXUJ
433 PAZLAE
434 BIQMET
435 PENTIM
436 PETCEW
437 PETWAN
438 PETWER
439 PIGRON
440 POFGUM
441 POTWOK
442 PUHSOB
443 PUJWIA
444 PUJWOG
445 NEGSOJ
446 BIWXEL
447 PUJWUM
448 PUNLEQ
449 PUZMAY
450 QABKAH
451 QABKIP
452 QACYAV
453 QANYUZ
454 QANZAG
455 QAWDEY
456 QAWFAX
457 BIWXIP
458 QAWLOR
459 QEDDIM
460 QEPHIC
461 QEPKUR

462 QEQHAV
463 QEQHID
464 QETKOQ
465 QEVBOI
466 QEZVOH
467 QEZVUN
468 BIXCEQ
469 QIDPAV
470 QIDPEZ
471 QIFKIA
472 QODDIW
473 QODDOC
474 QOWVAA
475 QOWVEE
476 QOXFOZ
477 QOXFUF
478 QOXGEQ
479 BIXDUH
480 QUBMIJ
481 QUBRIO
482 QUBYUH
483 QUBZAO
484 QUDWES
485 QUKTOF
486 QUMVUP
487 QUMVUP01
488 QUVRAB
489 RALRAX
490 BODNOY
491 RALVIJ
492 RAZDOM
493 REBNOB01
494 REMBER
495 REPQEI
496 RESFAW
497 REVHIJ
498 REVXEV
499 REWNAI
500 REWNEM
501 BOFGEJ
502 RIRCOL
503 RISZID
504 RIWLUF
505 ROCROQ
506 RODPUV
507 ROLXIA
508 ROPGUY
509 RUGGUW
510 RUMDOS
511 RUXCAO
512 BOKPAT
513 SADLUE
514 SAFFOW
515 SAKXAE
516 SALJUM
517 SALMAV
518 SAVCAV
519 SAWKUW
520 SAWMAG
521 SAWMEK
522 SAXCIE
523 BOLHUG
524 SAXWUK
525 SEQDIC
526 SESFAX
527 SIBWOP
528 SIGJAT
529 SIHHAT
530 SIKPEH
531 SIKZER
532 SIRRER
533 SOBTOS
534 BOLHUG01
535 SOMNIS
536 SONXIC
537 SOWSED
538 SOWSIH
539 SOWVOQ
540 SOWVUW
541 SOYPUR
542 SUKFOT
543 SULJOY
544 SUXTEK
545 BPYRUF
546 SUYGUP
547 TABTOH
548 TACWAW
549 TACWEA
550 TAHNIA
551 TAHNOG01
552 TAKJEW
553 TAKJUM
554 TAKKEX

555 TAKKIB
556 ACACRU02
557 BPYRUF01
558 TAPCOD
559 TARTEM
560 TAVVER
561 TAWDUQ
562 TETXEV
563 TEXCUV
564 TEXGEI
565 THAPRU
566 TIMCAT
567 TIPPOX
568 BPYRUF02
569 TIVQOE
570 TIWPEU
571 TOBQOQ
572 TOBQUW
573 TONKIQ
574 TOPLOA
575 TOSWIH
576 TURRII
577 TURROO
578 TUTSIK
579 BPYRUF10
580 TUTTEH
581 TUWNAB
582 TUXGUP
583 UCOFAU
584 UFEJUL
585 UFUQOB
586 UGAHEQ
587 UHALAR
588 UHOCAV
589 UJEGUM
590 BPYRUG
591 UJEHAT
592 UPOMUI
593 UQIMAJ
594 URICUU
595 UVUNIJ
596 UVUNOP
597 UZEFOV
598 VAHNAU
599 VANBES
600 VANTAH
601 BUQCIA
602 VASTUF
603 VAVFOO
604 VEFREE
605 VEFRII
606 VESZOI
607 VEYJOZ
608 VEYJUF
609 VIFRAD
610 VIKNOT
611 VIKNUZ
612 BUQGOJ
613 VIKPUB
614 VILSUE
615 VINZEX
616 VIRREU
617 VIWNAQ
618 VIWQAT
619 VOCCIA
620 VOCHAX
621 VOHKUY
622 VOQPOG
623 BZOCRU
624 VORHOZ
625 VORHUF
626 VOWDAM
627 VUGDOR
628 VUPKUM
629 VUXJUU
630 WABCEJ
631 WACWON
632 WACWUT
633 WALKAW
634 CAFHUO
635 WAQJIH
636 WAQREL
637 WAQRUB
638 WATLAE10
639 WATNOW
640 WATNUC
641 WATWUL
642 WATXOG
643 WAVDIH
644 WAWKUA
645 CAGSUY
646 WEDBIQ
647 WEFYEM

648	WEKTAI	679	CANDIE	710	YAJSIL
649	WEKYUG	680	XIFSAG	711	YAKKOM
650	WEKZAN	681	XIMWUM	712	CEJCUQ
651	WEMFOK	682	XIQHEL	713	YAKKUS
652	WEMFUQ	683	XIQHOV	714	YALVEM
653	WEMGAX	684	XIQHUB	715	YAPSIT
654	WESKAG	685	XITRIB	716	YAQSUE
655	WEVCEG	686	XIXFEP	717	YEDBUF
656	CAHWIR	687	XIXHIW	718	YEHNEE03
657	WILMOU	688	XIXHUI	719	YEHZAM
658	WIMJIM	689	XIXJAQ	720	YEJFIC
659	WIWNIZ	690	CEFCUM	721	YEMWUJ
660	WIWNOF	691	XIXJIY	722	YEMXOE
661	WIZZUA	692	XIXJOE	723	CEJLOS
662	WOBBEU	693	XONQAT	724	YIHCEY
663	WOBGEZ	694	XOZREJ	725	YIMJUZ
664	WOGJUY	695	XUBMOX	726	YISWEC
665	WONPAR	696	XUCXUO	727	YIYQIG
666	WOZZEQ	697	XUFTIC	728	YODXAQ
667	ACACRU03	698	XUHWAZ	729	YOFRUG
668	CAKQEK	699	XUHXUU	730	YOFSAN
669	WUNCAJ	700	XUQPOO	731	YOJROE
670	XAFJUJ	701	CEGBUL	732	YOJVUP
671	XAHZAJ	702	XUSJIE	733	YOJWAW
672	XASZIB	703	XUTWOY	734	CEJLUY
673	XAXCAB	704	XUWDEY	735	YOPDEM
674	XEDQAZ	705	XUXLAE	736	YOQJUK
675	XELWAM	706	YACMEV	737	YOZXIV
676	XEVSOG	707	YAHSOP	738	YOZXOB
677	XEZVED	708	YAHSOP10	739	YUSSUA
678	XEZVED01	709	YAJFAR	740	YUVWUH

741 ZACYOR
742 ZALGEY
743 ZAVFIN
744 ZEDRUV01
745 CENQUH
746 ZEDRUV02
747 ZEZMAS
748 ZIFLIJ
749 ZIJCUQ
750 ZIPGAG
751 ZIPGEK
752 ZIPGIO
753 ZIPGOU
754 ZIPHUB
755 ZISYEF
756 CHPYRU
757 ZISYIJ
758 ZOHZIF
759 ZOHZOL
760 ZUGBAG
761 ZUHZAD
762 ZUQNEE
763 ZUZSIW
764 CIGJUY
765 ACIDEW
766 CITDEP
767 CIYZIT
768 COBGAC
769 COCLAH
770 COCLAH10
771 COGXIG
772 COGXUS
773 COGYAZ
774 COKWOO
775 COKWUU
776 AFAVEI
777 COWQUA
778 CUHVAC
779 CUHWEH
780 CUHWIL
781 CYCPRU06
782 CYCPRU07
783 CYCPRU08
784 CYOCRU10
785 DABDEP
786 DABDIT